Structural Biology and Molecular Biophysics

Intraflagellar transport protein IFT172 contains a C-terminal ubiquitin-binding U-box-like domain involved in ciliary signaling

Reviewed Preprint
v1 • January 31, 2025
Not revised

Nevin K Zacharia, Stefanie Kuhns, Niels Boegholm, Anni Christensen, Jiaolong Wang, Narcis A Petriman, Anna Lorentzen, Jindriska L Fialova, Lucie Menguy, Sophie Saunier, Soren T Christensen, Jens S Andersen, Sagar Bhogaraju, Esben Lorentzen

Department of Molecular Biology and Genetics, Aarhus University, Aarhus, Denmark • Department for Biochemistry and Molecular Biology, University of Southern Denmark, Odense, Denmark • Department of Biology, University of Copenhagen, Copenhagen, Denmark • Laboratory of Hereditary and Kidney diseases, Institut Imagine, Paris, France • European Molecular Biology Laboratory, Grenoble, France

eLife Assessment

This **important** work advances our understanding of intraflagellar transport, ciliogenesis, and ciliary-based signaling, by identifying the interactions of IFT172 with IFT-A components, ubiquitin-binding, and ubiquitination, mediated by IFT172 C-terminus and its role in ciliogenesis and ciliary signaling. The results of the structural analysis of the IFT172 C-terminus and the evidence for the interaction between IFT172 and IFT-A components are **convincing**. However, the analysis of ubiquitin-binding and ubiquitination mediated by IFT172 is **incomplete**.

https://doi.org/10.7554/eLife.104906.1.sa4

Abstract

Intraflagellar transport (IFT) is a fundamental process driving ciliogenesis in most eukaryotic organisms. IFT172, the largest protein of the IFT complex, plays a crucial role in cilium formation and is associated with several disease variants causing ciliopathies. While IFT172 is tethered to the IFT-B complex via its N-terminal domains, the function of its C-terminal domains has remained elusive. Here, we reveal that the C-terminal part of IFT172 interacts with IFT-A complex subunits, providing a molecular basis for the role of IFT172 in bridging IFT-A and IFT-B complexes. We determine the crystal structure of the C-terminal part of IFT172, uncovering a conserved U-box-like domain often found in E3 ubiquitin ligases. This domain exhibits ubiquitin-binding properties and auto-ubiquitination activity. The IFT172 auto-ubiquitination activity is reduced in the C1727R patient ciliopathy variant. We use CRISPR-engineered RPE-1 cells to demonstrate that the U-box-like domain is essential for IFT172 protein stability and proper cilium formation. Notably, RPE-1 cells with heterozygous deletion of the U-box domain show altered TGFB signaling responses, particularly in SMAD2 phosphorylation levels and AKT activation. Our findings suggest a novel dual role for IFT172

in both structural support within IFT trains and regulation of ciliary ubiquitination and signaling pathways, providing new insights into the molecular mechanisms underlying IFT172-related ciliopathies.

Introduction

Cilia are hair-like microtubule (MT) based organelles that protrude from the cell surface of vertebrate cells and in several eukaryotic single-celled organisms. Cilia play indispensable roles in cellular motility, extracellular fluid flow, sensing extracellular cues, and coordinating cellular signaling pathways[1]. They are highly conserved from unicellular eukaryotes to humans and can vary greatly in length, copy number, and function. For example, in the unicellular algae *Chlamydomonas reinhardtii* (Cr), beating motions generated by motile cilia propel the cells through media[2]. Additionally, most vertebrate cells possess a single copy of non-motile primary cilia that performs sensory and signaling functions. The sensory capabilities of the primary cilium are attributed to ciliary coordination of signaling pathways such as TGF-beta (TGFB)/BMP, PDGF, and Hedgehog to drive organismal development and tissue homeostasis[3]. Aberrations to cilium assembly or function led to a class of human genetic disorders termed ciliopathies[4]. Ciliopathies affect a wide range of organs including the liver, kidney, and skeletal system and often manifest as syndromes such as Bardet Biedl syndrome and Meckel Gruber syndrome with overlapping phenotypes[5].

The proper assembly and function of cilia requires a bidirectional trafficking system known as intraflagellar transport (IFT)[6–8] to shuttle key ciliary components[9,10], including membrane-bound receptors such as G protein-coupled receptors (GPCRs) and ion channels that mediate signaling and sensory responses, between the cilium organelle and the cytoplasm[10–12]. IFT is carried out by the 23 subunit IFT complex that polymerizes into IFT trains[8,13] and traverses along the ciliary MT axoneme. IFT trains assemble at the ciliary base[14], associate with ciliary cargo[10,15] and undergo anterograde transport from the ciliary base to the tip powered by the Kinesin 2 motor[8,16]. A major remodeling of the anterograde IFT trains occurs at the ciliary tip[17], forming retrograde IFT trains that have a distinct ultrastructure[18], which subsequently traverse from the tip to the ciliary base powered by the Dynein 2 motor[19,20]. During the retrograde IFT, the IFT complex associates with the octameric BBSome complex to facilitate the targeted ciliary exit of several proteins[21,22]. The IFT trains are primarily understood to function as adaptors between the molecular motors and ciliary cargo to facilitate the dynamic localization of signaling components.

Ubiquitination is a well-studied posttranslational modification[23] that was recently shown to be crucial in ciliary homeostasis[24–26]. Ubiquitination is a multi-step enzymatic cascade where a ubiquitin molecule is shuttled from an E1 enzyme to the E2 enzyme and finally transferred to the substrate protein mediated by an E3 ligase[23]. Ubiquitination is known to be important in flagella disassembly in *Cr*[27]. Upon initiation of flagellar resorption, there is an upregulation of ubiquitination events, specifically that of tubulin subunits, facilitating ciliary disassembly[27,28]. Ubiquitination is also critical to ciliary signaling. The ciliary Hedgehog signaling pathway is a well-studied example of how regulatory ubiquitination events control signal dependent repression and activation of ciliary signaling[25,26,29,30]. In the absence of the Sonic Hedgehog ligand (SHH), the ciliary levels of the signal-transducing protein smoothened (SMO) is kept low for pathway repression[29]. This is achieved by the ubiquitination of SMO by the ciliary localized ubiquitin ligase wwp1, an event that subsequently targets SMO for IFT dependent ciliary exit[25,29]. Upon SHH binding, the ciliary exit of the ligand bound PTCH1 receptor and negative pathway regulator GPR161 occurs by the targeted ubiquitination of these receptors[26,30], leading to pathway activation. In the case of several GPCRs, such as GPR161 and SSTR3, signal dependent ciliary exit specifically relies on the ubiquitination of these receptors and subsequent IFT dependent ciliary exit[26]. Bonafide ubiquitin recognition domains are yet to

be identified in the IFT complex. Instead, the BBSome complex was shown to facilitate the recognition of these ubiquitinated GPCRs mediated by the TOM1L2 adaptor protein that harbors VHS and GAT domains capable of ubiquitin binding[31]. Moreover, a recent analysis of ubiquitinated proteins in the cilium of RPE1 cells identified signaling-related proteins to be enriched in the data set[32]. Specifically, components of the Wnt, Notch, and TGFB pathway were identified as targets of ciliary ubiquitination events. The BBSome complex, which mediates signal dependent ciliary exit of a wide array of ubiquitinated GPCRs, is in turn dependent on ubiquitination for proper assembly and function[33]. The cilium associated ubiquitin ligase PJA2 ubiquitinates the BBSome subunits BBS1 and BBS4, which is essential for normal BBSome assembly and ciliary GPCR trafficking[33]. Cilium associated ubiquitin ligases and ubiquitin binding domains thus emerge as crucial players in maintaining ciliary homeostasis.

IFT172 is the largest subunit in the IFT complex and is part of the IFT-B2 subcomplex[34]. The WD40 repeat containing N-terminal domain of the protein mediates interaction with the subunits IFT57 and IFT80, thereby maintaining IFT172 association with the IFT-B complex[34,35]. The C-terminal tetratricopeptide repeats (TPRs) of IFT172 remains rather uncharacterized in terms of structure and function despite the fact that IFT172 C-terminal variants have been detected in a cohort of ciliopathy patients with severe skeletal ciliopathy syndromes (Jeune syndrome and Mainzer-Saldino syndrome)[36]. Another cohort of patients with a milder ciliopathy resembling BBS also presented with IFT172 variations predominantly resulting in retinal defects[37]. Lastly, an isolated case of a patient exhibiting growth retardation was reported to have compound heterozygous IFT172 C-terminal mutations[38]. The importance of the IFT172 C-terminus is further exemplified by prior studies on various *in vivo* models. IFT172^{wim} mice carry a C-terminal point mutation (L1564P) causing major developmental defects and embryonic lethality caused by a complete loss of cilium in the embryonic node[39]. The Cr strain *fla11* carry the point mutation L1615P at the C-terminal TPRs of IFT172 resulting in flagellar resorption and IFT particle accumulation at the ciliary tip of green algae[40], a phenotype that was recapitulated in *Tetrahymena thermophila* models having progressive IFT172 C-terminal deletions[41]. Furthermore, it was observed that the Cr *fla11* strain accumulates ubiquitinated proteins in the cilium[42], which suggests that IFT172 could be involved in ciliary ubiquitination events. However, the molecular bases for these observations are currently not known.

In this study, we focused on structural and functional characterization of the IFT172 C-terminal region to reveal an interaction with IFT-A components and a very C-terminal ubiquitin-binding U-box domain that may regulate ciliary ubiquitination and signaling pathways.

Results

IFT172$_{968\text{-}C}$ interacts directly with subunits of the IFT-A complex

While the N-terminal β-propeller of CrIFT172 interacts with CrIFT57 and a central region (residues 626-785) interacts with CrIFT80, little is known about the function of the C-terminal 800 residues of IFT172. This region is predicted to fold into 20 TPRs followed by a small 70-80 residue domain of unknown function (**Fig. 1A**).

We purified a C-terminal construct of IFT172 (His-tagged CrIFT172$_{968\text{-}C}$) to homogeneity (**Fig. S1A**) and carried out pull-downs (PDs) from an extract of isolated Cr cilia (**Fig. S1B**). His-tagged Tobacco Etch Virus (TEV) protein was used as a negative control when detecting CrIFT172$_{968\text{-}C}$ interactors by mass spectrometry (MS) (**Figs. S1C-D**). Based on the resulting volcano plot (**Fig. S1C**, see also M&M), 10 proteins were annotated as interactors of CrIFT172$_{968\text{-}C}$ (**Fig. S1D**). Consistent with the fact that the CrIFT172$_{968\text{-}C}$ construct does not contain the IFT-B complex associating domains, no IFT-B proteins were found as interactors (**Fig. S1D**). Interestingly, however, several components of the IFT-A complex were identified as interaction

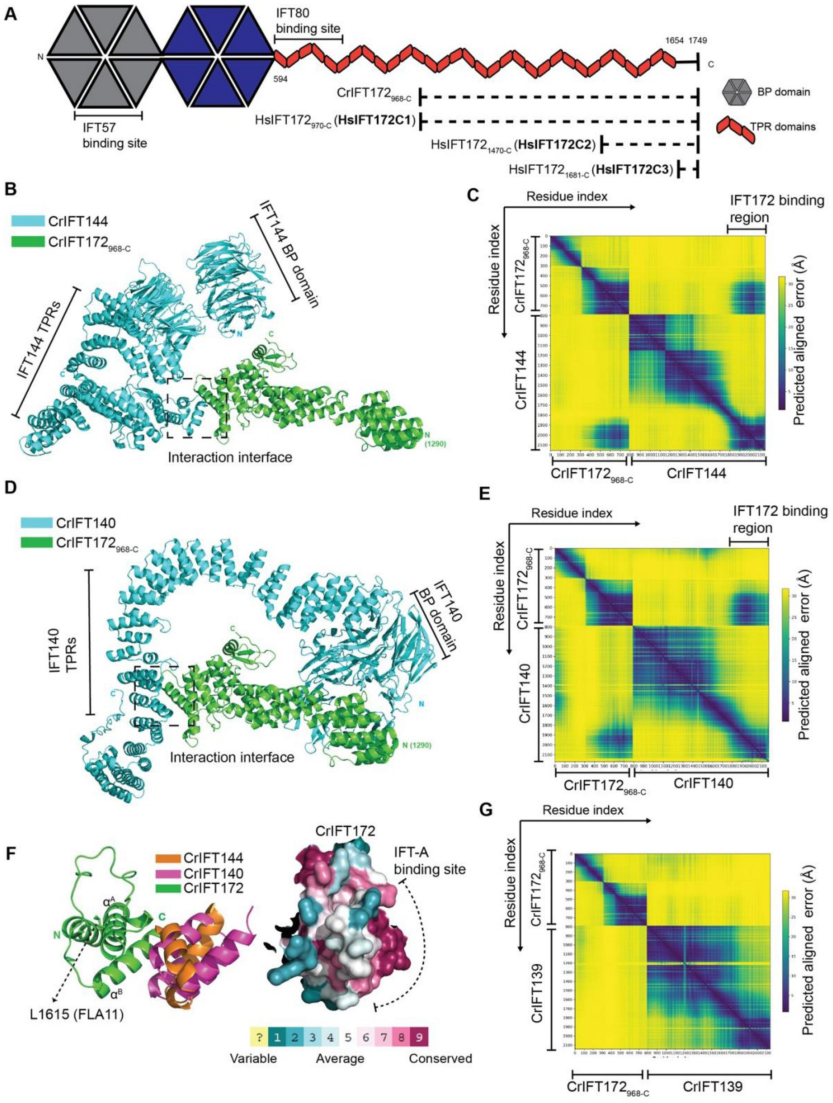

Figure 1.

The C-terminal TPRs of IFT172 constitute a binding site for IFT-A subunits.

(A) Schematic representation of Homo sapiens (Hs) IFT172 protein domain organization. β-propeller and TPR (tetratricopeptide repeat) domains are indicated. Solid lines represent previously identified IFT57 and IFT80 binding sites. Dashed lines show various truncated constructs of *Chlamydomonas reinhardtii* (Cr) IFT172 and HsIFT172 used in this study.
(B) Cartoon representation of the AlphaFold predicted structural model for a complex between $CrIFT172_{968\text{-}C}$ and CrIFT144. The interaction interface is highlighted.
(C) Predicted Aligned Error (PAE) plot for the AlphaFold model in panel B. X- and Y-axes show indexed residues from each protein used for PAE calculation. Low PAE scores indicate high confidence in the predicted interaction interface.
(D) Cartoon representation of the AlphaFold predicted structural model for a complex between $CrIFT172_{968\text{-}C}$ and CrIFT140, highlighting the interaction interface.
(E) PAE plot for the AlphaFold model in panel D, showing high confidence (low PAE values) for the interaction interface residue pairs.
(F) Left: Structural superposition of interaction interfaces from AlphaFold models in panels B and D. Subunits are colored as indicated. IFT144 and IFT140 are predicted to associate with an identical binding site formed by IFT172 TPR helices αA and αB. The L1615P temperature-sensitive mutation identified in the *fla11* strain of *C. reinhardtii* maps onto helix αA. Right: Surface amino acid conservation map for the IFT144/140 binding site in IFT172, color-coded as indicated.
(G) PAE plot for an AlphaFold predicted structure of the $CrIFT172_{968\text{-}C}$-CrIFT139 complex. High PAE scores for all inter-chain residue pairs suggest that IFT172 and IFT139 do not interact directly.

partners of CrIFT172$_{968\text{-}C}$ including IFT144, IFT140, and IFT139. Furthermore, a CH-domain containing protein of the central apparatus of the cilium as well as six additional proteins without a published ciliary localization were identified as IFT172 interactors (**Fig. S1D**).

To assess which of the 10 significant hits are direct interaction partners of CrIFT172$_{968\text{-}C}$, structural modeling using AlphaFold multimer (AF-M)[43,44] was carried out. This revealed 3 high-confidence hetero-dimeric complexes between CrIFT172$_{968\text{-}C}$ and each of the proteins: IFT144, IFT140, and a UBX-domain containing protein (uniprot: A0A2K3DQG3, CHLRE_06g293900v5) (**Fig. 1B-E** and **S1E-F**). None of the other seven candidate proteins, including IFT139 (**Fig. 1G**), was predicted with any confidence to interact directly with CrIFT172$_{968\text{-}C}$, and may constitute indirect interactors.

The structural model of the CrIFT172-IFT144 complex shows that the interaction is formed by the most C-terminal TPR of IFT172 (residues 1604-1669) and TPR helices of IFT144 (residues 1220-1250, see **Fig. 1B**). Surprisingly, the interaction with IFT140 (residues 1125-1162) utilizes the same TPR helices of CrIFT172 as the IFT144 interaction (**Fig. 1D** and **1F**). The structural models suggest that the interactions of IFT172 with IFT140 and IFT144 are mutually exclusive (**Fig. 1F**). Both IFT172-IFT144 and IFT172-IFT140 interactions are predicted with high confidence according to the Predicted Aligned Error (PAE) (**Figs. 1C** and **1E**). The conservation of the IFT140 and IFT144 interaction surface on IFT172 across ciliated organisms suggests a conserved function in binding IFT-A subunits (**Fig. 1F**).

We note that the IFT172 interacting helices of IFT144 are surface exposed in the cryo-EM structures of complete IFT-A complexes[45] and thus free to interact with IFT172 in IFT trains. Indeed, in the published cryo-ET structures of anterograde IFT-trains in Cr, the IFT172-IFT144 complex described here is observed[46]. Interestingly, cryo-ET structures of retrograde IFT trains demonstrate significant rearrangements of IFT-A and B sub-complexes[47] and reveal the same IFT172-IFT140 interaction as shown in **Fig. 1D-F**. The mutually exclusive interactions between IFT172 C-terminus and IFT140 or IFT144 thus underpin the different architectures of anterograde and retrograde IFT trains. **Fig. 1F** highlights the L1615 residue, which is mutated to a proline in the *fla11* strain resulting in a retrograde IFT defect phenotype in Cr[40] and accumulation of ubiquitinated proteins[42]. Interestingly, the L1615 residue is located in one of the two helices of IFT172 that interact directly with IFT140 or IFT144 (annotated as helix αA in **Fig. 1F**). This L1615P mutation will disrupt the helix αA, likely resulting in impaired binding of IFT172 to the IFT-A complex. This suggests that the molecular basis for the ciliary defects observed in *fla11* is caused by impaired IFT172-IFT-A association.

The uncharacterized UBX-domain-containing protein was validated by AF-M as a direct IFT172 interactor (**Fig. S1E-F**). UBX-domain-containing proteins generally function as cofactors that link the proteasome to ubiquitinated substrates, playing crucial roles in protein degradation and cellular quality control mechanisms[48]. They often act as adaptors, facilitating recognition and processing of ubiquitinated proteins by proteasomes. However, despite our interest in this potential interaction, we could not recombinantly express the UBX-domain-containing protein in a soluble form, which precluded further experimental characterization of its relationship with IFT172.

The crystal structure of human IFT172 reveals a C-terminal U-box-like domain

To gain deeper insights into the molecular architecture and potential functional domains of IFT172, we pursued crystallographic studies of IFT172C. Structural models of CrIFT172 predicted a small domain at the very C-terminus that does not form TPRs (**Fig. 2A**). This domain, which contains mixed α/β secondary structures, is linked to the IFT144 and IFT140 binding helices of IFT172 through a loop region (denoted as L0) that spans 30 residues. This arrangement places the

C-terminal domain roughly 25Å away from the IFT144 and IFT140 binding helices of IFT172 (**Fig. 2A**). In our pursuit of experimental validation, we isolated and crystallized a C-terminal construct of *Homo sapiens* (Hs) $IFT172_{1470\text{-}C}$ (hereafter referred to as HsIFT172C2, see **Fig. S2A** for purificaiton). This construct includes the IFT144 and IFT140 binding site and the small non-TPR C-terminal domain identified in the AlphaFold model of CrIFT172 (**Fig. 2A**). X-ray diffraction data were collected to 2.1Å resolution from native crystals and 2.8Å resolution at the peak wavelength of selenomethionine-substituted crystals (**Table 1**). Crystallographic phase information was obtained by combining molecular replacement (AlphaFold model of HsIFT172C2) and single-wavelength anomalous dispersion yielding an electron density map of excellent quality (**Fig. S2B**). This map allowed for the modeling of the entire structure, excluding a small loop (residues 1656-1657) and the seven most C-terminal residues. The crystal structure reveals that HsIFT172 contains a small domain (residues 1683-1749, referred to as HsIFT172C3) at the very C-terminus, which consists of a small 2-stranded β-sheet followed by two α-helices (see **Fig. 2B**). The preceding TPRs and connecting loop (loop L0, colored magenta in **Fig. 2B**) pack against this C-terminal domain via a central hydrophobic core and several peripheral polar interactions (**Fig. S2E**). Interestingly, numerous missense variants from ciliopathy patients[36–38] map to this interface and are highlighted in **Fig. 2B** as yellow sticks.

Using this C-terminal HsIFT172C3 domain structure in a DALI[49] search against the Protein Data Bank (PDB), structural similarities to RING domain-containing eukaryotic E3 ubiquitin ligase as well as possible prokaryotic RING domain homologues (Zinc finger proteins) were uncovered (**Fig. S2C**). RING domains are among the most abundant classes of ubiquitin ligase domain in humans[50]. Therefore, we sought to evaluate the possible structural similarity of HsIFT172C3 to various ubiquitin ligase domains. **Fig. 2C** presents a structural comparison of the HsIFT172C3 domain with representative domains from different classes of E3 ubiquitin ligases. HsIFT172C3 superposes with RING and U-box domains with root-mean-square deviations (RMSDs) of 2.0-2.6Å with structure-based sequence identities of 14-17% (**Fig. 2C** and **2F**). The common structural architecture of the U-box/RING domain is characterized by an N-terminal loop (L1) followed by a small two-stranded antiparallel β-sheet (β1 and β2), an α-helix (α1) and a C-terminal loop (L2) (**Fig. 2C**). The RING domain fold is stabilized by the coordination of two Zn^{2+} ions whereas the structurally and functionally similar U-box domain is instead stabilized by a network of polar contacts[51–53]. HsIFT172C3 has a U-box/RING domain structure with the important difference that L2 is replaced by an additional helix α2 (**Fig. 2C**). Interestingly, the CrIFT172 C-terminal domain is predicted to have the L2 loop and more closely resemble canonical U-box/RING domains (**Fig. 2A**). Upon inspecting the experimental electron density maps of HsIFT172C2, we did not observe any density at the corresponding Zn^{2+}-ion binding sites (see **Fig. 2D** for an anomalous electron density map). This observation is supported by sequence alignments, which show a lack of conservation of Zn^{2+} ion coordinating Cys and His residues in IFT172 proteins (**Fig. 2F**).

These observations suggest that IFT172C3 is not a classical RING domain but rather resembles a U-box domain. U-box/RING domains mechanistically function by binding the ubiquitin-loaded E2 enzyme (E2-Ub conjugate) thus restricting the E2-Ub conjugate to conformations that facilitate ubiquitin transfer to the substrate[54–57]. Interestingly, structural comparisons with well-characterized U-box domains indicate that the predicted E2 binding site in HsIFT172C3 is structurally occluded by TPRs preceding the U-box domain (**Fig. 2E**). Structural occlusion of the E2 binding site is a prominent mechanism of self-regulation seen in E3 ligases[58–61]. We conclude that IFT172 contains a U-box-like domain of unknown function at the very C-terminus, which is a hotspot for ciliopathy patient variants.

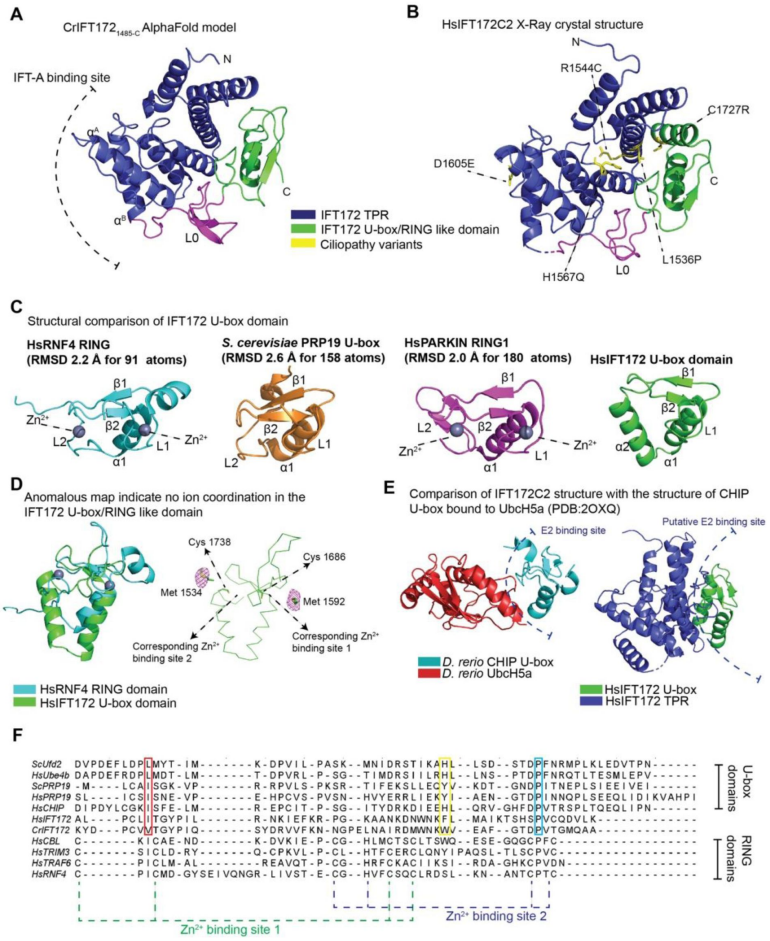

Figure 2.

IFT172 contains a U-box like domain distal to the IFT-A binding site.

(A) Cartoon representation of the AlphaFold-predicted structure of the C-terminal residues 1485-1755 of CrIFT172. This globular domain comprises several TPR helices, including the IFT140/144 binding αA and αB helices, followed by a loop region (L0) and a U-box/RING-like motif.
(B) Cartoon representation of the 2.1Å resolution X-ray crystal structure of HsIFT172C2. The structure exhibits a similar fold to the CrIFT172$_{1485\text{-}1755}$ AlphaFold model, composed of TPR helices followed by a loop region (L0) and a U-box/RING-like motif.
(C) Structural comparison of the U-box/RING-like motif in HsIFT172 with canonical RING domains of HsRNF4 (PDB: 4PPE), RING1 domain of PARKIN (PDB: 6HUE), and U-box domain of ScPRP19 (PDB: 6BAY), indicating the corresponding RMSD after superposition with the IFT172 motif. The U-box/RING-like motif in HsIFT172 superposes well with several structural components of U-box/RING domains, including the first loop (L1), the following beta strands (β1 and β2), and the helix (α1). A major difference in this HsIFT172 motif is the replacement of the characteristic second loop region (L2) found in U-box/RING domains with an alpha helix (α2).
(D) (Left) Structural superposition of the IFT172 U-box/RING-like domain with the RING domain of RNF4, identifying corresponding Zn^{2+} binding sites. Zn^{2+} ions in RNF4 are depicted as grey spheres. (Right) Anomalous density map represented as a magenta mesh contoured at 5σ, obtained from HsIFT172C2 selenium-methionine substituted protein crystals. Anomalous density depicted in proximity to the U-box/RING-like domain. Cys residues and neighboring Met residues in the predicted Zn^{2+} binding site of IFT172 are represented as sticks.
(E) (Left) Structure of the U-box domain in *D. rerio* CHIP bound to *D. rerio* UbcH5a (PDB: 2OXQ), indicating the E2 binding site on the CHIP U-box domain. (Right) Comparison of HsIFT172C2 crystal structure with PDB: 2OXQ indicates the putative E2 binding site on IFT172 U-box is occluded by the IFT172 TPR domain.
(F) Sequence alignment of U-box domains in HsIFT172 and CrIFT172 with several canonical U-box/RING domains. Zn^{2+} coordinating residues on RING domains are highlighted. Selected functionally relevant residues on U-box domains are depicted in boxes, and corresponding residues are also observed in the IFT172 U-box domain sequence.

Two protein copies / asymmetric unit	HsIFT172$_{1470\text{-}C}$ Native	*HsIFT172*$_{1470\text{-}C}$ Selenium methionine
Data collection		
Wavelength (Å)	1.006	0.9785
Resolution range (Å)	45.25-2.07 (2.10-2.07)	47.02-2.78 (2.95-2.78)
Space group	P 1 2_1 1	P 1 2_1 1
Unit cell (Å, °)	a = 46.97 b = 90.51 c = 67.42 α = 90 β = 97.42 γ = 90	a = 47.47 b = 90.63 c = 67.81 α = 90 β = 97.93 γ = 90
Total reflections	225982 (10379)	84456 (12152)
Unique reflections	34028 (1631)	26158 (3916)
Multiplicity	6.6 (6.4)	3.2 (3.1)
Completeness (%)	99.5 (96.2)	93.0 (85.9)
Mean I/sigma	9.7 (1.3)	8.3 (0.7)
Rpim	0.037 (0.483)	0.077 (1.65)
CC1/2	0.999 (0.777)	0.998 (0.494)
Refinement		
Resolution range (Å)	45.25-2.10 (2.17-2.10)	
Reflections for refinement	32556 (3050)	
Reflections for Rfree	1564 (151)	
Protein residues	532	
Number of atoms	4423	
Protein	24213	
Ligands	31	
Water (solvent)	179	
R-work	0.189 (0.367)	
R-free	0.238 (0.370)	
Ramachandran favored (%)	97.35	
Ramachandran outliers (%)	0.00	
RMS bonds (Å)	0.01	
RMS angles (°)	1.23	
Average B-factors (Å^2)	65.14	

Statistics for the highest resolution shell are shown in parentheses.

Table 1

X-ray diffraction data collection and refinement statistics (PDB: 9H2D).

IFT172 undergoes ubiquitination in the presence of the Ubch5a E2 enzyme

Given the structural similarity of HsIFT172C3 to U-box domains of well-characterized E3 ubiquitin ligases, we decided to test if IFT172 exhibits ubiquitination activity. To this end, various C-terminal constructs of Cr and Hs IFT172 proteins were tested in *in vitro* ubiquitination assays in the presence of purified MmUbe1 (E1 enzyme), ubiquitin, UbcH5a (E2 enzyme) and ATP (**Figs. 3A**). Appearance of ubiquitin conjugates were observed in reactions containing CrIFT172$_{968\text{-}C}$ and HsIFT172$_{970\text{-}C}$ (HsIFT172$_{970\text{-}C}$ will be referred to as HsIFT172C1 from hereon). In the presence of ubiquitination pathway components (E1, E2, and ATP), ubiquitin ligases have the characteristic property of self-ubiquitination (auto-ubiquitination) *in vitro*[53,62]. Screening activity for HsIFT172C1 with 11 different E2 enzymes revealed the appearance of ubiquitin conjugates only in the presence of members of the Ubch5 E2 enzyme family (**Fig. 3B**). The molecular mass of the ubiquitin conjugate is consistent with mono-ubiquitinated HsIFT172C1 used in the assay (**Fig. 3A** and **3B**) and is also stained by anti-His antibodies detecting the His-tag on HsIFT172C1 (**Fig. 3C**). Polyubiquitination is a hallmark of E3 ubiquitin ligases resulting in an observed smear of ubiquitinated products on ub-antibody stained western blots[53]. A characteristic smear is not observed in the case of IFT172 but rather a strong band corresponding to mono-ubiquitination is observed. The low *in vitro* ubiquitination activity exhibited by IFT172 may potentially be attributed to structural inhibition as the IFT172 U-box interface involved in E2 binding is occluded in the HsIFT172C2 crystal structure (**Fig. 2E**). Interestingly, higher molecular weight ubiquitinated bands of lower intensity, that migrates close to the prominent mono-ubiquitinated IFT172 are observed in several replicates (**Fig. 3A**, 3B and 3F). These bands could potentially correspond to additional mono-ubiquitination events on IFT172 or the formation of short poly-ubiquitin chains on IFT172.

Additional control experiments show that ubiquitin conjugates are only formed in the presence of all ubiquitination pathway components (E1, E2, ATP and ubiquitin) but not observed when WT UbcH5a is replaced by a catalytically dead mutant (**Fig. 3D**). Furthermore, the observed HsIFT172C1 ubiquitin conjugates disappear upon incubation with the Usp2 deubiquitinase enzyme and the HsIFT172C1 ubiquitin conjugate is resistant to reducing SDS-PAGE analysis (**Fig. S3A** and **B**). Combined, these observations indicate a canonical lysine-linked ubiquitin conjugation occurring on HsIFT172C1 in the presence of UbcH5a, possibly in coordination with the IFT172 U-box domain.

We were unable to test the Ub-box domain alone as the untagged HsIFT172C3 construct did not yield soluble protein expression. We did obtain protein expression for a GST-tagged HsIFT172C3 construct but several proteolytically cleaved fragments co-purified suggesting that the Ubox domain was partly degraded (**Fig. S4B**). Neither this GST-tagged HsIFT172C3 nor the HsIFT172C2 protein showed any ubiquitination activity (**Fig. 3A**). However, the longer CrIFT172$_{968\text{-}C}$ and HsIFT172C1did show auto-ubiquitination activity (**Fig. 3A**). Therefore, ubiquitination of HsIFT172 requires TPRs located N-terminally of the TPRs present in the crystallized construct shown in **Fig. 2B**, likely providing the ubiquitin accepting lysines.

We note that, unlike the canonical U-box/RING domain-containing proteins, IFT172 does not exhibit strong poly-ubiquitination activity *in vitro*. Moreover, Ubch5 proteins are highly reactive and often exhibit E3-independent ubiquitin transfer activity[63] and it is thus possible that the observed IFT172 ubiquitination is a result of U-box-independent Ubch5 activity. As deletion of the U-box domain rendered IFT172 constructs insoluble in *E. coli*, we pursued mutagenesis studies on the U-box domain in context of the HsIFT172C1 construct. A common method to inactivate U-box/RING domains is to disrupt E2 binding[64]. Comparisons of the IFT172 sequence (**Fig. 2F**) and structure (**Fig. 3E**) with well-characterized U-box domains indicated two potential E2 binding residues in the IFT172 U-box domain. This includes a highly conserved Ile/Leu residue

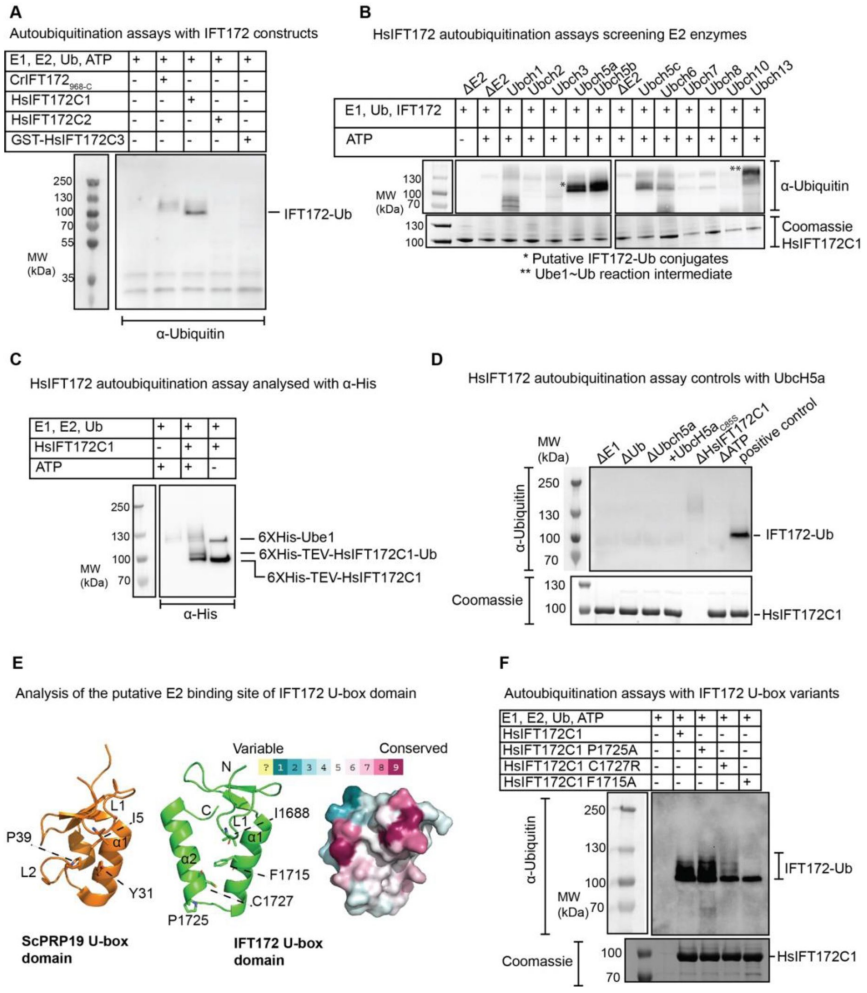

Figure 3.

IFT172 exhibits ubiquitin conjugation activity in the presence of UbcH5a.

(A) Western blot analysis of an *in vitro* auto-ubiquitination assay containing *M. musculus* Ube1(E1), HsUbcH5a (E2), Ubiquitin (Ub) and ATP in the presence of various C-terminal IFT172 constructs as potential E3 ligases. Reactions were visualized by immunostaining with anti-Ubiquitin antibody.
(B) Western blot analysis of *in vitro* autoubiquitination assays containing Ube1 (E1), Ub, ATP and HsIFT172C1, in the presence of 11 different ubiquitin-conjugating E2 enzymes (Abcam #ab139472). Reactions were visualized by immunostaining with (top) anti-Ubiquitin antibody and (bottom) Coomassie staining. Reactions were conducted under non-reducing conditions, accounting for the visualization of significant amounts of E1~Ub conjugate in the blot.
(C) *In vitro* auto-ubiquitination assays containing *M. musculus* 6XHis-Ube1, 6XHis-TEV-HsUbcH5a, Ub and 6XHis-TEV-HsIFT172C1. Reactions were visualized by immunostaining with an anti-His tag antibody.
(D) Western blot analysis of *In vitro* auto-ubiquitination reactions containing *M. Musculus* Ube1(E1), HsUbcH5a (E2) WT/C85S mutant, Ubiquitin (Ub), HsIFT172C1 and ATP. As specified in each reaction, a reaction component was omitted (indicated by Δ) or a mutant component was used instead of the corresponding WT component (indicated by +). Reactions were visualized by immunostaining with (top) anti-Ubiquitin antibody and (bottom) Coomassie staining.
(E) Analysis of the putative E2 binding site in the (center) HsIFT172 U-box domain and (Left) U-box domain of ScPRP19. Both U-box domains are shown facing the E2 binding site. The PRP19 residues I5, Y31, and P39 whose mutagenesis leads to the loss of its ubiquitin ligase activity are represented as sticks (also highlighted in boxes within the sequence alignment in **Fig. 2E**). The equivalent residues in the putative E2 binding site of IFT172 are also depicted as sticks. (Right) Surface amino acid conservation map for the E2 binding site in IFT172 U-box domain, color-coded as indicated.
(F) Western blot analysis of *in vitro* ubiquitination assay with HsIFT172C1 WT and the specified HsIFT172C1 U-box variants. Reactions were visualized by immunostaining with (top) anti-Ubiquitin antibody and (bottom) Coomassie staining.

(I1688 in HsIFT172) in loop L1 of U-box/RING domains[51,64] (**Fig. 3E** and highlighted with a red box in **Fig. 2F**) involved in E2 binding. Secondly, a conserved aromatic residue (F1715 in HsIFT172) is commonly found in helix α1 of U-box/RING domains[51,65] (**Fig. 3E** and highlighted with a yellow box in **Fig. 2F**) where it contributes to E2 binding. Finally, a completely conserved proline residue is found in the loop L2 of U-box domains[51,53] (P1725 in HsIFT172, see **Fig. 2F** and **3E**), which in IFT172 caps the N-terminus of alpha-helix α2. Mutation of this conserved proline residue results in a complete loss of ubiquitination activity for four different U-box domain-containing proteins[53]. Interestingly, the IFT172 ciliopathy variant C1727R[36] also maps to helix α2 in the U-box domain (**Fig. 3E**). Notably, I688 and F1715 are located near an evolutionarily conserved surface patch on the putative E2 binding site of IFT172 (**Fig. 3E**). To test the importance of these residues in IFT172 auto-ubiquitination, the residues Ile1688, Phe1715 and Pro1725 in IFT172 were mutated to alanine, whereas Cys1727 was mutated to arginine to mimic the patient variant. Soluble protein expression was obtained for each of the F1715A, P1725A, and C1727R HsIFT172C1 variants (but not for the I1688A variant) and the soluble proteins were purified (**Fig. S3C-F**). *In vitro* ubiquitination assays show that while mono-ubiquitination is not affected in IFT172 mutants, significant loss of the higher molecular weight bands for ubiquitinated IFT172 was observed for the F1715A and C1727R variants (**Fig. 3F**). IFT172 ubiquitination activity is thus affected by mutations of the putative E2 binding site of IFT172 U-box domain. We note that the strong mono-ubiquitination of IFT172 observed in **Fig. 3F** is likely U-box-independent ubiquitination by the E2 enzyme as this activity is not affected by IFT172 U-box mutations. In summary, we conclude that IFT172 exhibits auto-ubiquitination activity that is reduced in E2-binding and ciliopathy variants of IFT172.

IFT172 U-box domain interacts directly with ubiquitin *in vitro*

To further assess the biochemical properties of IFT172, we carried out interaction studies of HsIFT172C2 with stable mimics of the E2~Ub (UbcH5a~Ub) conjugate. To this end, the UbcH5a active site cysteine was mutated to a serine, which allowed for the production and purification of a stable oxyester-linked UbcH5a~Ub conjugate[66], which mimics the native thioester-linked E2-Ub conjugate (**Fig. S4C**). Interactions between IFT172 and the UbcH5a~Ub conjugates were analyzed by affinity pulldowns using GST-tagged HsIFT172C2 (**Fig. 4A**) showing an interaction between IFT172C2 and the WT UbcH5a~Ub conjugate. Additionally, we produced and tested two point-mutants of the UbcH5a~Ub conjugate (UbcH5a F62A or A96D) known to disrupt interaction with U-box/RING domains[67–69]. However, these mutations did not prevent the interaction between UbcH5a~Ub and HsIFT172C2 (**Fig. 4A**). Moreover, structural modeling of a hetero-dimeric complex between HsIFT172C3 and UbcH5a using AF-M did not indicate a direct interaction (**Fig. 4B**). *In silico* screening of complex formation between IFT172C3 and each of the 40 annotated Hs E2 enzymes also did not reveal confident complex formation with any of the E2 enzymes (data not shown). Combined, this indicates that although IFT172 associates with the E2-Ub conjugate in PDs, this association may not be mediated by direct interactions with the E2 enzyme (**Fig 4A**).

Alternatively, the interaction between IFT172 and UbcH5a~Ub could be mediated through ubiquitin. Indeed, several crystal structures have elucidated the RING-E2~Ub interaction, demonstrating direct interactions between the RING domain and ubiquitin[55,56,58]. Given that E2 mutations do not abolish the interaction between UbcH5a~Ub and HsIFT172C2, we reasoned that the interaction could be mediated by ubiquitin. N-terminally linked tetra-ubiquitin chains were pulled down with GST-tagged HsIFT172C2 indicating an IFT172-ubiquitin interaction (**Fig. 4C**). To test if the conserved IFT144 and IFT140 binding site on IFT172 is involved in ubiquitin binding, a pull-down was carried out with tetra-ubiquitin with the HsIFT172C2_D1605R mutant. Asp1605 corresponds to a previously reported human ciliopathy locus[37] that maps onto the corresponding IFT144 and IFT140 binding site on IFT172. This HsIFT172C2_D1605R mutation does not appear to influence the binding to ubiquitin (**Fig. 4C**). Pulldown of the tetra-ubiquitin chain with GST-tagged HsIFT172C2 or HsIFT172C3 indicates that both constructs pulldown tetra-ubiquitin at comparable levels (**Fig. 4D**). This suggests that the U-box domain is the ubiquitin-

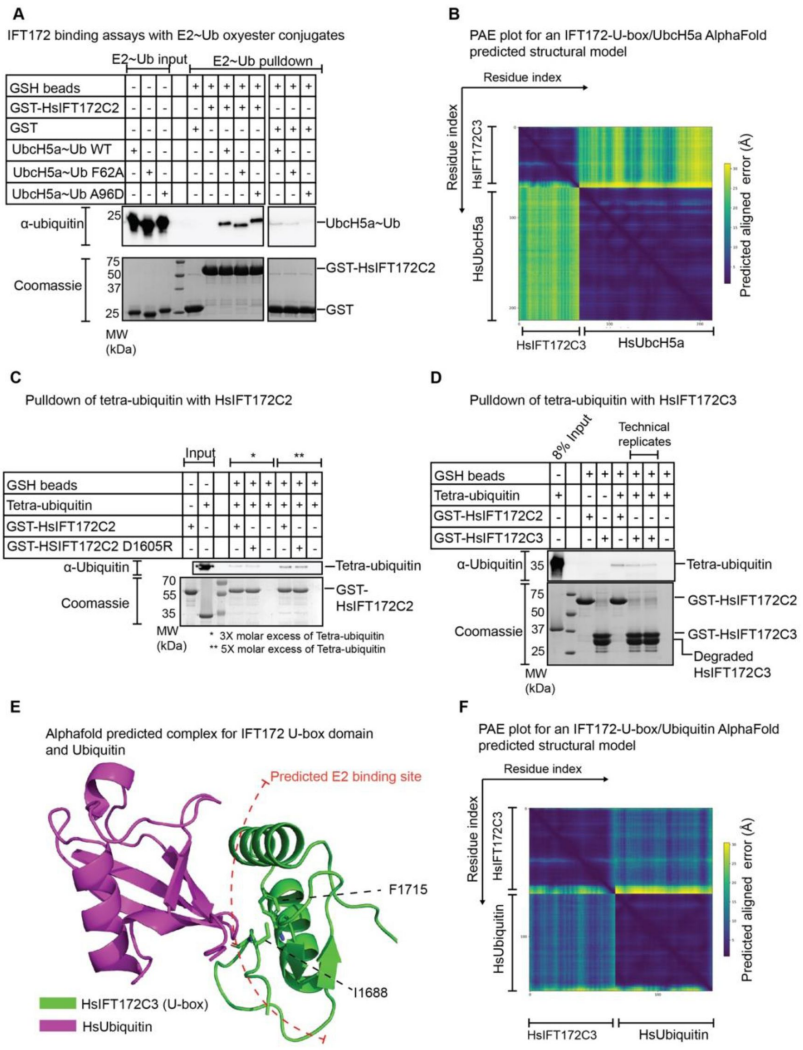

Figure 4.

IFT172 U-box domain is a binding site for ubiquitin.

(A) Pulldown of purified UbcH5a$_{C85S}$~Ub conjugates with GST-tagged HsIFT172C2 immobilized on GSH beads. Samples after elution were analyzed by western blotting with (top) anti-ubiquitin antibody and (bottom) Coomassie staining. Input shown is 2% for the western blot and 7.8% for the Coomassie staining.
(B) PAE plot for an AlphaFold-generated structural model for a complex between HsIFT172C3 and HsUbcH5a. High error values are observed for interchain residue pairs, suggesting no high confidence prediction for an interaction between the two chains.
(C) Pulldown of tetra-ubiquitin with GST-tagged HsIFT172C2 constructs immobilized on GSH beads. The D1605R mutation on the IFT-A binding site of HsIFT172C2 does not impact the binding of tetra-ubiquitin to HsIFT172C2. Reactions were visualized by immunostaining with (top) anti-ubiquitin antibody and (bottom) Coomassie staining.
(D) Pulldown of tetra-ubiquitin with various GST-tagged HsIFT172 constructs immobilized on GSH beads. Both HsIFT172C2 and HsIFT172C3 pulldown tetra-ubiquitin at similar levels. The prominent lower molecular weight band in the HsIFT172C3 sample is a degradation/proteolytic cleavage product obtained upon HsIFT172C3 expression and purification from *E. coli*. The two lanes showing a pulldown of tetra-ubiquitin with HsIFT172C3 represent technical replicates. Reactions were visualized by immunostaining with (top) anti-Ubiquitin antibody and (bottom) Coomassie staining.
(E) AlphaFold-predicted structural model for a complex between HsIFT172C3 and HsUbiquitin. The model suggests that ubiquitin binds to the predicted E2~Ub binding site of HsIFT172C3. The predicted E2 binding residues of the HsIFT172 U-box domain are depicted in the model.
(F) PAE plot for the AlphaFold structural model shown in panel E. Moderate PAE scores are observed for the residue pairs corresponding to the interaction interface (panel E) between the two chains.

binding site. Indeed, AF-M modeling of the IFT172 U-box domain with ubiquitin suggests the formation of a complex between the IFT172 U-box and ubiquitin (**Fig. 4E-F**). It was previously reported that E2 enzymes catalyze the E3-independent mono-ubiquitination of proteins containing a ubiquitin-binding domain[63]. It is thus possible that the mono-ubiquitination of HsIFT172C1 observed in the presence of UbcH5a (**Fig. 3**) could be a result of the ubiquitin-binding capability of HsIFT172C1. Nevertheless, the bands corresponding to additional ubiquitination events on HsIFT172C1 (**Fig. 3F**) could be attributed to a potential E3 ligase activity of HsIFT172. Therefore, the biochemical characterizations of IFT172 presented here (**Figs. 3** and **4**) indicate that IFT172 may have both a ubiquitin-binding and conjugation activity.

Loss of IFT172 U-box domain impairs protein stability and leads to ciliogenesis defects in RPE1 cells

To investigate the cilium-specific functions of the U-box domain of IFT172, we used CRISPR/Cas12a to engineer human RPE1 cell lines carrying a deletion of the IFT172 U-box domain. A schematic and nomenclature for the four generated RPE1 cell lines are shown in **Fig. 5A**. Ciliogenesis in these cells was induced by serum withdrawal for 24h and cilia were visualized by staining for acetylated tubulin. In cells with a homozygous IFT172 U-box domain deletion cilia formation was severely reduced compared to cells expressing GFP-tagged full-length IFT172 (**Fig. 5B**). Moreover, cilia that are retained in the IFT172ΔU-box (homozygous) cells are significantly shorter, with a median cilia length of ~1.3 μm in IFT172ΔU-box (homozygous) cells, compared to ~3.0 μm in IFT172-FL (homozygous) cells (**Fig. 5B**). Meanwhile, in cells with a heterozygous IFT172 U-box domain deletion no significant effect on ciliation or ciliary length was observed (**Fig. 5B**). To further investigate the observed ciliogenesis phenotype, the localization of the eGFP-tagged IFT172 proteins were analyzed by immunofluorescence microscopy. Both the full-length IFT172 protein as well as the IFT172ΔU-box truncation were recruited to the cilium (**Fig. 5C**). The full-length IFT172 protein is present along the length of the axoneme, with notable accumulations at the ciliary base and tip. In the cells with a homozygous IFT172 U-box deletion, eGFP-tagged IFT172ΔU-box protein is accumulated along the short axoneme, but in heterozygous cells that form normal length cilia, the distribution of the eGFP-tagged IFT172ΔU-box protein is similar to the full-length IFT172 protein (**Fig. 5C**). This consistent localization pattern suggests that the U-box domain is not essential for IFT172 trafficking to or within the cilium, despite its impact on overall protein levels and ciliogenesis.

Examination of protein expression levels using immunostaining revealed a striking reduction in the levels of the U-box deleted IFT172 protein (**Fig. 5D**). The specific IFT172 antibody used here was generated against an HsIFT172 epitope (amino acids 1353-1652) that lies outside the U-box domain. The reduced detection of IFT172 is thus most likely due to reduced protein expression or stability levels upon U-box deletion. As IFT172 is known to be essential for ciliogenesis[41,70], the severe reduction in expression levels of both IFT172 alleles causes ciliogenesis defects in the IFT172ΔU-box (homozygous) cells. Meanwhile, in the IFT172ΔU-box (heterozygous) cells, the observed upregulation in the WT IFT172 allele compensates for the reduced expression levels of the U-box truncated IFT172 allele (**Fig. 5D**), which likely provides sufficient IFT172 for ciliogenesis at a similar level as the parental RPE1 cells (**Fig. 5B**). However, the IFT172ΔU-box protein contains both IFT-A and IFT-B binding sites required for incorporation into IFT trains and the IFT172ΔU-box (heterozygous) cells will thus have a reduction in the concentration of IFT172 with a U-box domain as compared to parental cells.

IFT172 U-box domain influences TGFB signaling

Given that the U-box deleted IFT172 still localizes to the cilium (**Fig. 5C**), we wanted to investigate if ciliary signaling events are impacted by the loss of the IFT172 U-box domain. The severe ciliogenesis defects exhibited by the IFT172ΔU-box (homozygous) cells (**Fig. 5B**) will result in U-box-independent secondary effects that may affect signaling responses. Therefore, we focused our attention on the IFT172ΔU-box (heterozygous) cells that possess normal ciliation and

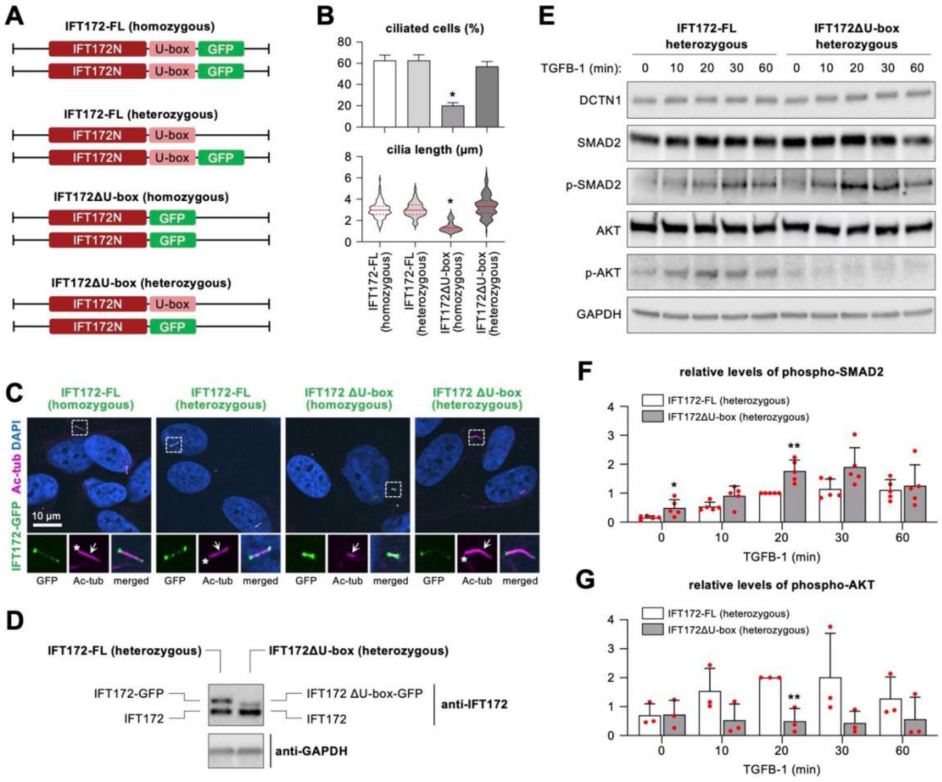

Figure 5.

Truncation of the IFT172 U-box domain impairs ciliogenesis and leads to altered TGFB signaling response in RPE1 cells.

(A) Schematic representation and nomenclature of RPE1 cell lines generated by CRISPR/Cas12a-mediated exon targeting of the IFT172 gene.
(B) Quantification of ciliogenesis (percentage of ciliated cells, upper panel) and ciliary length (lower panel) in all RPE1cell lines. Error bars in the upper panel represent standard error of the mean (*: p<0.05).
(C) IFM analysis of IFT172-GFP (*green*) localization to primary cilia (acetylated tubulin (Ac-tub., *red*) in RPE1 cell lines. Nuclei are stained with DAPI (*blue*). The top row displays whole-cell views, while the bottom row panels show zoomed in insets of the cilium (arrows). Asterisks indicate ciliary base region.
(D) WB analysis of IFT172 expression in IFT172-FL (heterozygous) and IFT172ΔU-box (heterozygous) RPE1 cell lines.
(E) WB analysis of phosphorylation levels of SMAD2 (p-SMAD2) and AKT (p-AKT; p-AKT^{T308}) in IFT172-FL (heterozygous) and IFT172ΔU-box (heterozygous) RPE1 cell lines treated with 2 ng/mL TGFB-1 ligand for the indicated time points.
(F,G) Quantification of p-SMAD2 (F) and p-AKT (G) levels from panel E, normalized to DCTN1 and GAPDH. Error bars represent standard error of the mean (*: p<0.05; **:p<0.01).

initially investigated TGFB signaling in these mutant cells. To this end, previous studies showed that the primary cilium regulates both canonical and non-canonical branches of TGFB signaling[71,72] the former operating through activation of R-SMAD transcription factors at the ciliary pocket, where ciliary receptors are internalized for phosphorylation of SMAD2/3[71]. Compared to control cells, IFT172ΔU-box (heterozygous) cells showed an increased level of SMAD2 activation upon TGFB-1-stimulation, and the level of SMAD2 phosphorylation also appeared slightly elevated in unstimulated heterozygous IFT172ΔU-box cells (**Fig. 5E-F**). In contrast, TGFB-1-mediated activation of AKT, which operate in the non-canonical branch of TGB signaling, was markedly reduced in heterozygous IFT172ΔU-box cells (**Fig. 5E** and **5G**). We further evaluated AKT activation in response to PDGF-DD stimulation, which activates the homodimer of PDGFRB outside and independent of the primary cilium[73]. In this case, PDGF-DD induced activation of AKT was unaffected in the heterozygous IFT172ΔU-box cells (**Figs. S5A-B**). Thus, perturbation to the IFT172 U-box domain results in differential effects on TGFB-mediated signaling pathways, for which the U-box domain may play a regulatory role in the mechanisms by which the cilium balances the output of canonical versus non-canonical TGFB pathways.

Discussion

IFT172 bridges IFT-A and IFT-B complexes in IFT trains

This study provides new insights into the structure and function of IFT172, a key component of the intraflagellar transport machinery. The N-terminal region of IFT172 is known to form inter-IFT subunit interactions with the IFT-B subunits IFT57/IFT80[34,35,74], while much less was known about the C-terminal part of IFT172. Our comprehensive structural and biochemical analyses reveal two functionally relevant motifs at the C-terminus of IFT172: a TPR motif involved in IFT-A association and a U-box-like domain likely involved in ciliary ubiquitination events. These discoveries not only enhance our understanding of the role of IFT172 in IFT but also suggest new mechanisms for the regulation of ciliary function.

Early studies on IFT172 hypothesized a function in anterograde to retrograde transition of IFT trains at the ciliary tip[40]. This hypothesis was based on the observation that the Cr *fla11* strain with a C-terminal missense mutation in IFT172 leads to an accumulation of IFT proteins at the ciliary tip, a phenotype characteristic of retrograde IFT defects[40]. Our findings now provide a molecular basis for the retrograde IFT phenotype observed in the *fla11* strain. We show that the FLA11 mutation lies in the TPR motif of IFT172 directly associating with IFT subunits IFT144 and IFT140 (**Fig. 1** and **S1**). This suggests that impairment of the association of IFT172 with IFT-A likely underlies the faulty switch to retrograde IFT. Our results align with recent cryo-ET structures of anterograde and retrograde IFT trains, which show that the IFT172 C-terminus interacts with IFT144 in anterograde trains and with IFT140 in retrograde trains[46,47].

Interestingly, the human ciliopathy variant D1605E[37] also localizes to the corresponding IFT-A interaction site in the *Hs*IFT172, suggesting that impaired IFT-A association contributes to disease manifestation. Collectively, these findings establish IFT172 as a key IFT subunit that bridges IFT-B and IFT-A complexes in both anterograde and retrograde IFT trains, providing a molecular basis for its involvement in ciliopathies.

Stoichiometry and potential ubiquitin-related functions of IFT172 in IFT trains

Recent cryo-EM reconstructions of IFT trains have revealed a stoichiometry of 2:1 for IFT-B to IFT-A complexes[46,47]. This stoichiometry implies that only half of the IFT172 C-termini are engaged with IFT-A, while the remainder are potentially free to interact with other ciliary components. Our discovery of a U-box-like domain in IFT172 (**Fig. 2**), and the identification of a

UBX domain protein as an interaction partner, suggests potential ubiquitin-related functions for IFT172 within the cilium. These functions could extend beyond proteasomal degradation to include roles in ubiquitin-mediated protein trafficking or regulation. This hypothesis is supported by our observation of weak *in vitro* auto-ubiquitination activity of IFT172 (**Fig. 3F**), although *bona fide* ciliary ubiquitination substrates remain to be identified.

The IFT172 U-box domain appears to be in an auto-inhibited state in our crystal structure of HsIFT172C2 (**Fig. 2E**), potentially explaining the relatively weak observed activity. This structural inhibition is reminiscent of the RING ubiquitin ligase CBL[59], where phosphorylation and substrate binding trigger a conformational change that activates ligase activity[59,75]. Intriguingly, the phosphosite database[76] lists four residues (T1533, S1549, T1689, Y1691) at the U-box/TPR interface as phosphorylation sites (**Fig. S2D**). Phosphorylation of these residues could potentially alleviate the auto-inhibited state, suggesting a possible regulatory mechanism. Furthermore, a 30-residue linker connects the U-box domain to the last TPR of IFT172, likely providing significant conformational flexibility (**Fig. 2A-B**). This flexibility may be functionally crucial for the U-box domain, allowing it to adopt different conformations as needed for its various roles.

Our biochemical characterization has further revealed ubiquitin-binding properties of IFT172, mapped to the U-box-like domain (**Fig. 4**). While this property is atypical for U-box domains, it bears resemblance to structurally related zinc finger domains, such as the UBZ domain with a β-β-α motif[77]. These domains function as ubiquitin-binding domains (UBDs) regulating various cellular processes[77]. This finding is particularly intriguing as RING domains, which are structurally similar to U-box domains, are known to mediate contacts with ubiquitin for priming the E2-Ub conjugate for ubiquitin transfer[55,56].

The ubiquitin-binding capability of IFT172 could facilitate the trafficking or turnover of ubiquitinated proteins in the cilium, complementing known ubiquitin-dependent processes. For instance, signal-dependent ciliary exit of ubiquitinated GPCRs and the Hedgehog pathway component Smoothened[25,29] is mediated by UBDs in the adaptor protein TOM1L2[26,31]. However, UBDs associated with several other cilium-associated signaling pathways and processes are yet to be identified. While IFT139 has been implicated in the ciliary turnover of ubiquitinated tubulin during ciliary disassembly[28], unlike TOM1L2, ubiquitin-binding sites have not been validated in IFT139 or any other BBSome or IFT subunits. This positions the IFT172 U-box domain as a potential UBD for the trafficking or turnover of ubiquitinated proteins in the cilium.

Implications of the IFT172 U-box domain in ciliary signaling

Several ciliopathy variants map to the C-terminal part of IFT172[36–38] and are located in the vicinity of the U-box domain (**Fig. 2B**). These mutations could disrupt ubiquitin-related functions of the U-box domain or impair protein stability. To investigate the physiological relevance of the IFT172 U-box domain, we analyzed engineered RPE1 cells with U-box deletions. While homozygous deletion of the U-box domain significantly impaired total IFT172 protein levels and affected ciliogenesis, a heterozygous deletion maintained near-wild-type levels of total IFT172 protein and cilium formation (**Fig. 5B-D**). In the heterozygous U-box deleted cells, we observed altered SMAD2 phosphorylation levels (**Fig. 5E-F**) and impaired AKT activation (**Fig. 5E** and **G**) in response to TGFB-1 stimulation. These findings suggest that the U-box domain is crucial for protein stability and its deletion differentially affects the SMAD and non-SMAD TGFB activation pathways. The final phenotypic outcome of TGFB signaling depends on the balance and fine-tuning of both SMAD and non-SMAD activation pathways, as these pathways engage in extensive cross-talk and can mutually regulate each other[78–80]. Our results suggest that IFT172, through its U-box domain, may play a crucial role in maintaining this balance.

The mechanism behind this regulation likely involves the trafficking and processing of TGFB pathway components. Recent proteomic studies have shown that many endocytosis-related proteins are enriched in the ciliary ubiquitinome[32], suggesting that receptor trafficking and processing within the cilium are highly regulated by ubiquitination. Given our findings that IFT172 possesses both ubiquitin-binding and potential ubiquitin ligase activities, we propose that IFT172 could directly influence the fate of ubiquitinated TGFB receptors. This function would be particularly relevant at the ciliary base and tip, where major sorting decisions occur. The altered signaling responses in U-box mutants could result from changes in receptor residence time, internalization rates, or trafficking routes within the cilium.

In conclusion, our findings reveal that IFT172, beyond its structural role in IFT trains, has an unexpected function in signal regulation. The flexible nature of half of the IFT172 C-termini in IFT trains, combined with its ubiquitin-related activities, positions IFT172 as a potential master regulator of ubiquitin-mediated processes within the cilium. This dual functionality - providing both structural support and signaling regulation - may explain why IFT172 mutations lead to such diverse ciliopathy phenotypes. These results expand our understanding of how IFT proteins contribute to ciliary signaling beyond their established roles in protein transport.

Materials and Methods

Cloning and expression of proteins in *E.coli*

DNA sequences encoding the respective truncations of HsIFT172 and CrIFT172 as well as full length HsUbiquitin and HsUbcH5a were Polymerase Chain Reaction (PCR) amplified. Gibson assembly[81] was used to insert the genes into pEL_A or pEL_K vectors with either N-terminal 6XHis-TEV or 6XHis-GST-TEV tags. Mutations were introduced by PCR of the corresponding plasmids. Plasmids were transformed into *E. coli* BL21 (DE3) and the cells were grown at 37°C in TB medium supplemented with appropriate antibiotics to an OD_{600} of 1. After cooling down the culture to 18°C, protein expression was induced by addition of 0.5 mM Isopropyl β-d-1-thiogalactopyranoside (IPTG). Cells were harvested after overnight protein induction at 18°C.

Protein purification

Cell pellets were resuspended in four times the pellet volumes of lysis buffer (50 mM Tris pH 7.5, 300 mM NaCl, 10% glycerol, 5 mM β-mercaptoethanol) supplemented with 1 mM phenylmethanesulfonyl fluoride (PMSF) and SM DNAse. The cells were lysed by sonication and clarified by ultracentrifugation at 74000 relative centrifugal force (RCF) for 30 minutes. The cleared lysate was loaded onto a Ni^{2+}- NTA column (5 ml, Roche) prewashed with lysis buffer. After loading the lysate, the column was further washed with 8 Column volumes (CV) of lysis buffer, 8 CV QB buffer (20 mM Tris pH 7.5, 1 M NaCl, 10% glycerol, 5 mM β-mercaptoethanol) and 8CV of QA buffer (20 mM Tris pH 7.5, 50 mM NaCl, 10% glycerol, 5 mM β-mercaptoethanol) supplemented with 20 mM Imidazole. The proteins were eluted from the Ni^{2+}-NTA column by passing QA buffer containing 250 mM imidazole. The eluted proteins were loaded onto a HiTrap Q HP 5 ml anion exchange column (GE Healthcare) pre-equilibrated with QA buffer. Elution from the Q column was performed by a 0-100% gradient from QA to QB buffer. The elutions containing the proteins were loaded onto a HiLoad 16/600 Superdex 75 or HiLoad 16/600 Superdex 200 column (GE Healthcare) pre equilibrated with SEC buffer (10 mM HEPES pH 7.5, 150 mM NaCl, 1 mM Dithiothreitol (DTT)).

For the purification of His-GST-TEV-HsIFT172$_{1681\text{-}C}$, His-MmUbe1, His-TEV-HsUbcH5a, His-TEV-(Tetra-ubiquitin) and His-Strep-TEV-HsUbiquitin the cell lysates over expressing the proteins were prepared as above. After loading the clarified lysate onto the Ni^{2+}-NTA column, the column was washed with 8CV of lysis buffer, 8 CV of QB buffer and 8CV of QA2 buffer (20mM Tris pH 7.5, 100mM NaCl, 10% glycerol, 5 mM β-mercaptoethanol) supplemented with 20mM Imidazole.

Proteins were eluted by passing 20mL QA2 buffer containing 250mM Imidazole followed by 20mL of QA2 buffer containing 500mM Imidazole. The purest elutions were dialyzed overnight in SEC buffer and afterwards loaded on a HiLoad 16/600 Superdex 75 or HiLoad 16/600 Superdex 200 column (GE Healthcare) pre-equilibrated with SEC buffer. Selenomethionine substituted HsIFT172C2 protein was expressed in BL21 Star cells and grown in M9 medium with addition of amino acids. The protein was purified as described above.

Culturing and flagella isolation of Cr

CrCC-1690 strain was obtained from the Chlamydomonas Resource Center (*https://www.chlamycollection.org*). The cells were maintained on solid Agar plates consisting of standard tris acetate phosphate (TAP) media in a sterile environment at room temperature with a table lamp as a continuous light source. Cells for flagella extraction were grown in two flasks each with 4L of (TAP) media for 3 days at room temperature with a table lamp as continuous light source. Cells were grown to an OD_{700} of 0.4. The cultures were harvested and dibucaine induced flagella abscission and subsequent flagella isolation was carried out as reported in Craige et al., 2013[82]. The isolated flagella were solubilized overnight at 4°C in solubilization buffer (10mM HEPES pH 7.5, 5 mM $MgSO_4$, 4% Sucrose, 25mM KCl, 10mM β-mercaptoethanol, 0.3% IGEPAL 630) supplemented with protease inhibitor (Roche #05892791001). Afterwards, the axonemal fraction of the flagella lysate was pelleted by centrifugation of the flagella lysate at 45,000 RCF for 30min at 4°C. The supernatant containing the IFT proteins and motor proteins were used for subsequent pulldowns with $CrIFT172_{968\text{-}C}$.

Affinity pulldowns

For the pulldown with Cr flagella extracts, 30μM of His-$crIFT172_{968\text{-}C}$ or 30μM His-TEV protease were immobilized on 50μL of TALON beads (GE healthcare #28-9574-99) by incubation at 4°C for 1 hour. Afterwards the beads were washed 3 times with HMSK buffer (10mM HEPES pH 7.4, 5mM $MgSO_4$, 4%(w/v) sucrose and 25mM KCl) to remove unbound proteins. 1mg Cr flagella extract diluted in 300μL HMSK buffer was incubated with the beads at 4°C for 2 hours. After incubation, beads were washed three times with HMSK buffer containing 30mM Imidazole and bound proteins were eluted in HMSK buffer containing 300mM Imidazole.

For the GST pulldowns 10μM of the GST tagged protein or GST tag were immobilized on 10 μL GSH beads (Cytiva #17-5279-01) by incubation for 1 hour at 4°C with constant mixing. Beads were washed once with PD buffer (50mM Tris pH 7.5, 100mM NaCl and 1mM DTT) to remove unbound proteins. Prey proteins were diluted in 100μL PD buffer and incubated with the beads at 4°C for 2 hours. The beads were washed three times with PD buffer and bound proteins were eluted in elution buffer (10mM HEPES pH7.5, 100mM NaCl, 30mM Reduced glutathione and 1mM DTT). The specific amount of prey proteins supplied were 20μM UbcH5a~Ub in the pulldown shown in **Fig. 4A**, 25μM tetra-ubiquitin in the pulldown shown in **Fig. 4D**. For the pulldown shown in **Fig 4C**, 5μM of immobilized GST-HsIFT172C2 was incubated with 15μM or 25μM tetra-ubiquitin as specified. PD elutions were visualized by Coomassie staining and western blotting with anti-ubiquitin (Merck, #05-944, 1:5000) antibody after separation on an SDS-PAGE gel.

Ubiquitination assays

Auto-ubiquitination assays with purified UbcH5a as E2 were performed in a 50 μL reaction volume. The reaction contained 0.1 μM E1 (His-MmUbe1), 2.5 μM E2 (His-TEV-UbcH5a), 10 μM ubiquitin (R&D Systems #U-100H-10M) and 2 μM of the specified His-TEV-HsIFT172C constructs. Reactions were initiated by addition of 5 mM ATP and incubated at 37°C for 1.5 hours in ubiquitination buffer (50 mM Tris pH 7.5, 50 mM NaCl, 5 mM $MgCl_2$ and 0.5 mM DTT). The reactions were stopped by addition of equal volumes of 2X SDS-PAGE loading buffer (100 mM Tris pH 6.8, 10% v/v β-mercaptoethanol,4% v/v SDS, 0.2% v/v bromophenol blue, 20% v/v glycerol).

Reactions were later visualized by Coomassie staining and western blotting with anti-ubiquitin (Merck,#05-944, 1:5000) antibody or anti-His (GeneScript, #A00186, 1:5000) antibody after separation on an 8% SDS-PAGE gel.

For the E2 enzyme screen shown in **Fig. 3B**, 20 µL reactions were set up containing 0.25 µM E1 (His-MmUbe1), 2.5 µM of the specified E2 enzyme (Abcam #ab139472), 5 µM ubiquitin (R&D Systems #U-100H-10M) and 2 µM His-TEV-HsIFT172C1. The reactions were initiated by addition of 5 mM ATP and carried out in ubiquitination buffer (Abcam #ab139472) supplemented with 5 mM $MgCl_2$. The reactions were incubated at 37°C for 1.5 hours. The reaction was stopped by addition of equal volumes of 2X non-reducing SDS-PAGE loading buffer (Abcam #ab139472). Reactions were analyzed by Coomassie staining and western blotting with anti-ubiquitin antibody (Merck, #05-944, 1:5000) after separation on a 4-15% gradient SDS-PAGE gel.

The protocol for generating the UbcH5aC85S~Ub conjugate (**Fig. S4C**), was adapted from Middleton et al., 2014[66]. Briefly, a 5 mL *in-vitro* charging reaction was set up containing MmUbe1, $UbcH5a_{C85S}$, ubiquitin (recombinantly purified with an N-terminal 6XHis-Strep-TEV tag) and ATP. The charging reaction was incubated overnight at 30°C to achieve maximal UbcH5aC85S~Ub formation, followed by separation on a HiLoad Superdex 75 SEC column.

Cell culture

Adherent hTERT-immortalized Retinal Pigment Epithelial 1(RPE1) cells were grown in Dulbecco's Modified Eagle Medium F12 (DMEM/F-12, GlutaMAX Supplement (Gibco #31331-093)) containing 1% penicillin-streptomycin (Sigma-Aldrich #P0781) and 10% fetal bovine serum (FBS Gibco #10438-026) at 37°C, 5% CO_2 and 95% humidity. Cells were passaged twice a week. Cells were serum starved for 48 hours prior to ligand stimulation by replacing the culture media with DMEM F12 containing 1% Penicillin-Streptomycin.

Ligand stimulation assays

Serum starved RPE1 cells and fibroblasts were stimulated by addition of respective serum starvation media containing 2ng/mL TGFB-1 ligand (R&D Systems #240B) for the specified time points. The stimulation was quenched by washing the cells with ice cold Phosphate-Buffered Saline (PBS) (137mM NaCl, 2.7mM KCl, 10mM Na_2HPO_4 and 1.8mM KH_2PO_4) followed by addition of lysis buffer. M-Per Lysis buffer (ThermoScientific #78501) supplemented with protease inhibitor (Merck #05056489001) and anti-phosphatase (ThermoScientific #1862495) was used for quenching and cell lysis. Lysates were centrifuged at 20000 RCF for 20 min at 4°C and the supernatant was stored at -20°C. Samples were later analyzed by western blots with antibodies as indicated. Antibodies used in western blots are listed in **Table 2**.

Crystallization, X-ray diffraction data processing and structure determination

HsIFT172C2 was crystallized by vapor diffusion by mixing 200 nL of purified protein at a concentration of 2.4 mg/ml mixed with an equal volume of precipitant solution containing 0.2 M Sodium phosphate dibasic dihydrate, 20% w/v Polyethylene glycol 3350, pH 9.1. Crystals were transferred to the cryo-protectant containing the precipitant solution supplemented with 10% glycerol before freezing. X-ray diffraction data were collected at the Swiss Light Source (SLS; Villigen, Switzerland) at the PXII beamline on a Pilatus 6M detector and indexed/integrated with the XDS package[83] before scaling with Aimless as part of the CCP4 package[84]. Molecular replacement using the AlphaFold generated model for HsIFT172C2 was carried out in the program Phaser[85] as available in the software packages PHENIX[86]. Molecular replacement identified two molecules of $HsIFT172_{1470\text{-}C}$ in the asymmetric unit. Single anomalous dispersion diffraction data collected at the Selenium peak wavelength on Selenium methionine substituted protein

Protein	Primary antibody catalogue No.	Primary antibody dilution	Secondary antibody catalogue No.	Secondary antibody dilution
ubiquitin	Merck #05-944	1:5000	Dako #P0161	1:1000
His tag	Genscript #A00186	1:5000	Dako #P0161	1:1000
IFT172	Santa Cruz #Sc398393	1:200	Agilent #P0447	1:10000
p-SMAD2	Cell Signaling #3108s	1:500	Agilent #P0399	1:10000
p-AKT^{T308}	Cell Signaling #2965s	1:500	Agilent #P0399	1:10000
p-AKT^{S473}	Cell Signaling #4060s	1:500	Agilent #P0399	1:10000
SMAD2	Cell Signaling #5339s	1:200	Agilent #P0399	1:10000
AKT	Cell Signaling #9272s	1:500	Agilent #P0399	1:10000
DCTN1	BD Transduction laboratories #610474	1:500	Agilent #P0447	1:10000
GAPDH	Cell Signaling #14C10	1:1000	Agilent #P0399	1:10000

Table 2

List of primary and secondary antibodies used in western blots

crystals were combined with the molecular replacement solution in Phaser to produce phase information to calculate the map shown in **Fig. S2B**. Given this map, the AutoBuild function in PHENIX was utilized for model building yielding initial R_{work}/R_{free} values of 0.30/0.35. This was followed by iterative cycles of manual model building in Coot[93] and refinement in PHENIX using torsion angle non crystallographic symmetry and secondary structure restraints as well as translation libration screw (TLS) refinement, to yield a final model with an R_{work}/R_{free} of 0.195/0.240 (see **Table 1**).

Mass Spectrometry based fragment identification for CrIFT172$_{968\text{-}C}$ interactors

Samples were prepared using the SP3 protocol[87] with reduction, alkylation, and trypsin digestion. Peptides were labeled with TMT6plex (ThermoFisher) and fractionated by high pH reverse phase chromatography. LC-MS/MS analysis was performed on an UltiMate 3000 RSLC nano LC system coupled to an Orbitrap Fusion Lumos Tribrid Mass Spectrometer. Full scan MS1 (375-1500 m/z) was acquired at 60,000 resolution, followed by data-dependent MS2 scans at 15,000 resolution. Data were processed using IsobarQuant and Mascot (v2.2.07) against the Chlamydomonas reinhardtii proteome (UP000006906). Fixed modifications were Carbamidomethyl (C) and TMT10 (K); variable modifications were Acetyl (Protein N-term), Oxidation (M), and TMT10 (N-term). Mass tolerances were 10 ppm for MS1 and 0.02 Da for MS2. Quantification required at least two unique peptides per protein. Data analysis was performed in R, using limma for batch correction and vsn for normalization. Differential expression was assessed using limma, with hits defined as having FDR < 5% and fold-change ≥ 100%, and candidates as FDR < 20% and fold-change ≥ 50%.

CRISPR-mediated endogenous tagging of IFT172 in RPE1 cells

The CRISPR/Cas12a-assisted PCR tagging approach was used to endogenously tag IFT172 with eGFP in RPE1 cell line as previously described[88] Briefly, HDR repair templates were produced by PCR with target-specific primers containing the homology arms and the plasmid pMaCTag-P05 (Addgene plasmid 120016)[89] In addition to the homology arms and the eGFP sequence, the HDR repair template also encodes a puromycin cassette for selection and an expression cassette for a Cas12a crRNA. For tagging full-length IFT172 (IFT172-FL) at its C-terminus, the Cas12a crRNA (5'-CCTTTCAGTAGTTGGTAGAG-3') targeted the IFT172 locus at the stop codon, and the homology arms were designed to insert the eGFP sequence before the stop codon. To generate the deletion of the IFT172 U-box domain (IFT172 ΔU-box), the homology arms were designed to insert the eGFP sequence after amino acid 1688, and the target sequence of the corresponding Cas12a crRNA (5'-TTACAGGTATAGAAGCCTAC-3') spanned the intended integration site. Doxycycline-inducible RPE1 cells expressing the CRISPR nuclease enAsCas12a[90] were electroporated with HDR repair template using the Neon Transfection System (ThermoFisher Scientific). After the transfection, the cells were treated for three days with the DNA-PK inhibitor M3814 to increase the knock-in efficiency[91] and subsequently selected with puromycin for 2 weeks, to isolate single cell clones. The clonal cell lines were screened for successful tagging by live cell imaging and PCR. In this study four cell lines were used (**Fig. 5A**). 1: IFT172-FL (homozygous): Both alleles contained the eGFP insert at the C-terminus before the stop codon. 2: IFT172-FL (heterozygous): One allele contained the eGFP insert at the C-terminus, the other allele was the unaltered wildtype allele. 3: IFT172 ΔU-box (homozygous): U-box domain deleted in both alleles by the insertion of eGFP after amino acid 1688. 4: IFT172 ΔU-box (heterozygous): U-box domain deleted in one allele; the other allele was the unaltered wildtype allele. Correct knock-in and the absence of indels was confirmed by Sanger sequencing.

Immunofluorescence staining and microscopy

RPE1 cells were grown on glass coverslips to 70-80 % confluency and serum-starved for 24 h to induce ciliogenesis. Cells were fixed with 3% PFA in PBS for 15 min and permeabilized for 5 min in 0.2% Triton X-100/PBS. Blocking was performed for 30 min with 3% BSA in PBS. A mouse monoclonal antibody against acetylated tubulin (Sigma-Aldrich, Clone 6-11B-1, diluted 1:500) was used to stain for the ciliary axoneme. For protein localization studies, GFP fluorescence was visualized directly. Primary antibodies were diluted in blocking solution and incubated with the cells at room temperature for 2 h or at 4°C overnight. Coverslips were washed three times with PBS and incubated with an anti-mouse secondary antibody conjugated to Cy3 (Jackson Immuno Research Labs, Cat# 715-165-150, diluted 1:500) for 1 h at room temperature. DAPI (40,6-diamidino-2-phenylindole, Sigma-Aldrich) was included with secondary antibodies for DNA staining. Coverlsips were washed three times with PBS and mounted on glass slides in Mowiol (Sigma-Aldrich).

Widefield images were acquired as z-stacks at 0.3 µm intervals using a Zeiss AxioImager M1 microscope equipped with a Zeiss CellObserver equipped with an Apochromat 63×/NA1.4 oil-immersion objective and a CoolSNAP HQ2 camera. Confocal images were acquired as z-stacks at 0.125 µm intervals using a Nikon Ti-2, A1 LFO confocal microscope with a Plan Apo λ 100× NA 1.4 oil objective. Image analysis was performed using Fiji/ImageJ (NIH)[92]. For quantification of ciliation frequencies, maximum intensity projections of z-stacks were generated, and the number of nuclei/cells and cilia were determined using DAPI and acetylated tubulin staining, respectively. For ciliary length measurements, the region of interest was manually defined using the line segment tool. Measurements were obtained from four independent experiments, and 30-60 cells were analyzed per condition and replicate. Graphs were drawn, and statistical analysis was performed using Prism (GraphPad). Data are presented as mean +/- standard error of the mean (SEM) or box-and-whisker plots with horizontal lines showing 25, 50 and 75th percentiles and whiskers extending to minimum and maximum values.

AlphaFold

All structural models not supported by crystallographic data were predicted using a local installation of AlphaFold v. 2.3.2[43-44]. Visualizations of protein structure was done using PyMOL v. 2.5 (Schrodinger LLC, *https://pymol.org*).

Note

This reviewed preprint has been updated to include a co-corresponding author.

Figures and figure legends

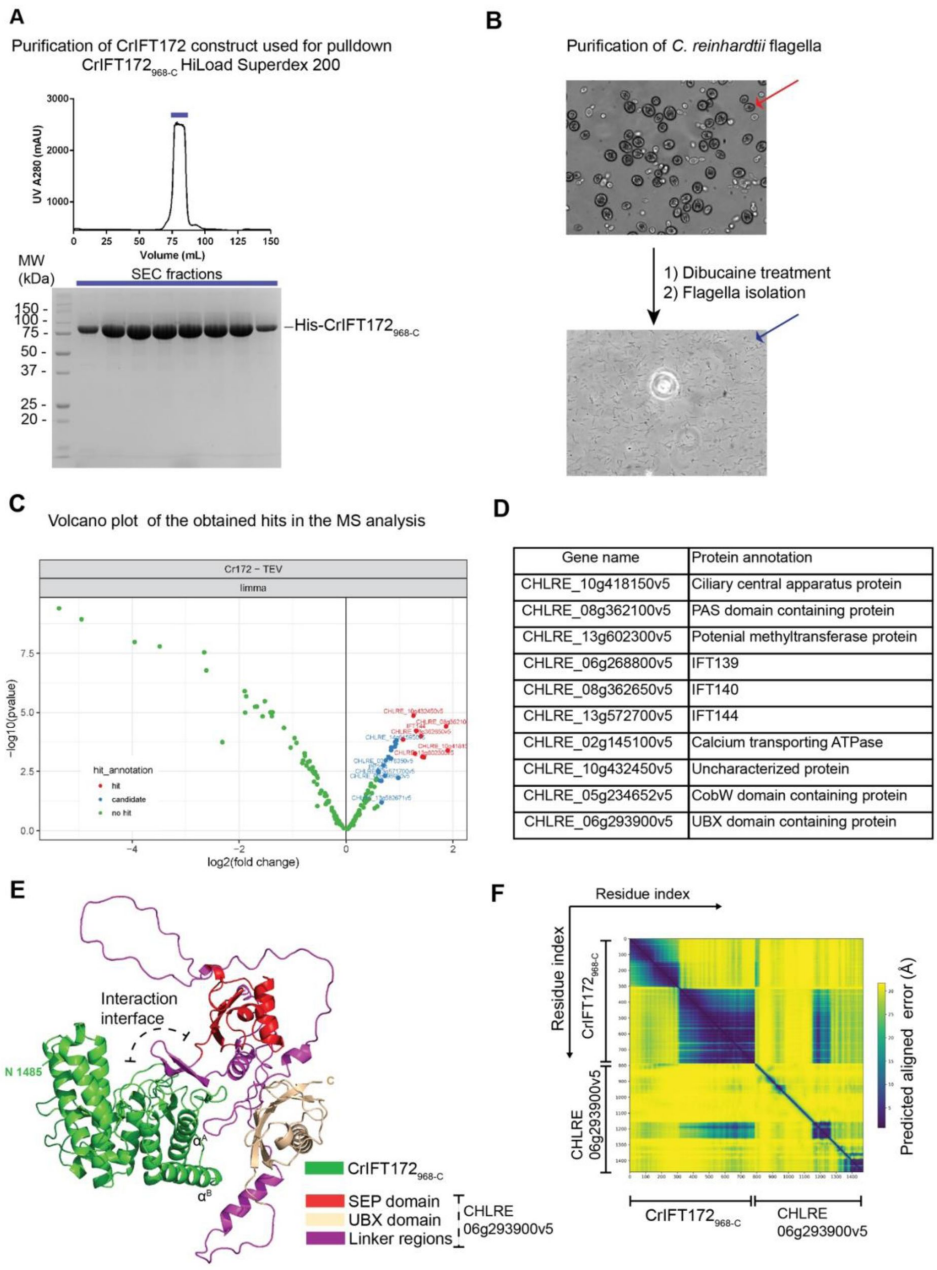

Gene name	Protein annotation
CHLRE_10g418150v5	Ciliary central apparatus protein
CHLRE_08g362100v5	PAS domain containing protein
CHLRE_13g602300v5	Potenial methyltransferase protein
CHLRE_06g268800v5	IFT139
CHLRE_08g362650v5	IFT140
CHLRE_13g572700v5	IFT144
CHLRE_02g145100v5	Calcium transporting ATPase
CHLRE_10g432450v5	Uncharacterized protein
CHLRE_05g234652v5	CobW domain containing protein
CHLRE_06g293900v5	UBX domain containing protein

Figure S1.

Uncovering interactors of the CrIFT172 C-terminus

(A) Size exclusion chromatography (SEC) elution profile for CrIFT172$_{968\text{-}C}$ (top). Protein composition of denoted elution fractions analyzed by Coomassie staining after SDS-PAGE separation (bottom).
(B) *Chlamydomonas reinhardtii* CC1690 cells visualized by light microscopy before flagella isolation (top) and purified flagella fraction after de-flagellation at the same magnification (bottom).
(C) Volcano plot showing distribution of mass spectrometry (MS) analysis hits for flagellar proteins pulled down by CrIFT172$_{968\text{-}C}$ in *C. reinhardtii* CC1690, compared against the tobacco etch virus (TEV) protease control.
(D) Table of the 10 significant CrIFT172$_{968\text{-}C}$ flagellar interactors identified in panel C. Gene name(left) and protein annotations from Uniprot (right) are shown.
(E) Alphafold predicted structural model for a complex between CrIFT172$_{968\text{-}C}$ and the UBX domain containing protein (CHLRE_06g293900v5) identified as an interaction partner (**Fig. S1C-D**). A linker region that lies between the UBX and SEP domains is predicted to form contacts with IFT172. The IFT-A binding helices described in **Fig. 1F** are denoted as α^A and α^B.
(F) PAE plot for the AlphaFold predicted structure shown in panel E.

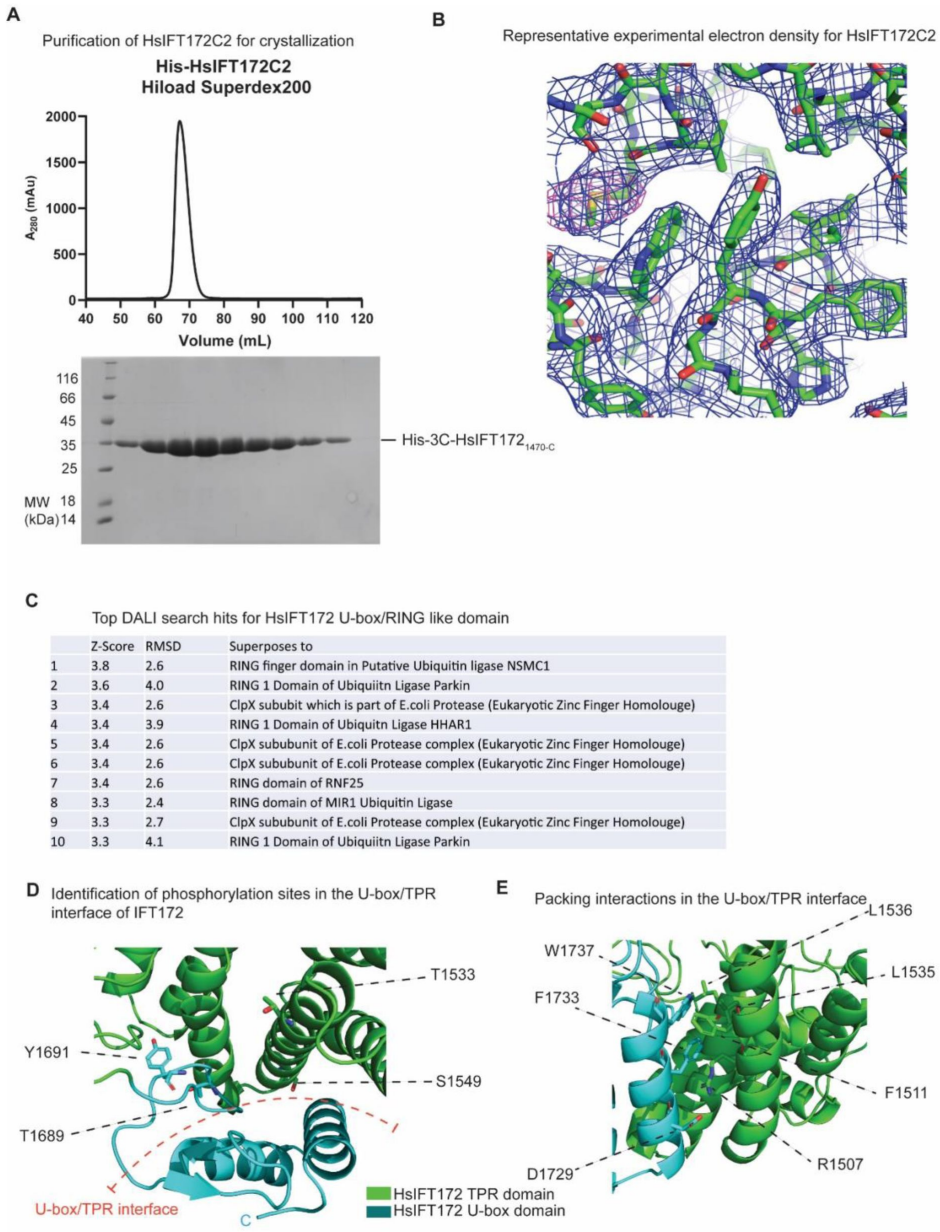

Figure S2.

Purification and structure determination of HsIFT172 C-terminal domain.

(A) SEC elution profile for HsIFT172C2 shown on top. The protein composition of the denoted elution fractions was analyzed by Coomassie staining on an SDS-PAGE (bottom).
(B) Representative electron density map for HsIFT172C2 crystals. The MR-SAD map is shown as a blue mesh contoured at 1σ and SeMet anomalous density is shown as a magenta mesh contoured at 5σ.
(C) Top 10 hits obtained from a search of structural homologs for HsIFT172C3 against the PDB database using the DALI server[49]. Z-score and RMSD of corresponding structural alignment are indicated.
(D) Phosphorylation sites on HsIFT172C2 identified from curated databases of known phosphorylation sites[76]. The phosphorylation sites on HsIFT172C2 are exclusively present at the TPR/U-box interface, suggesting phosphorylation as a potential mechanism for relieving the structural inhibition of the U-box E2 binding site.
(E) Representative hydrophobic and polar contacts that allow the IFT172 U-box domain to pack against the TPR helices.

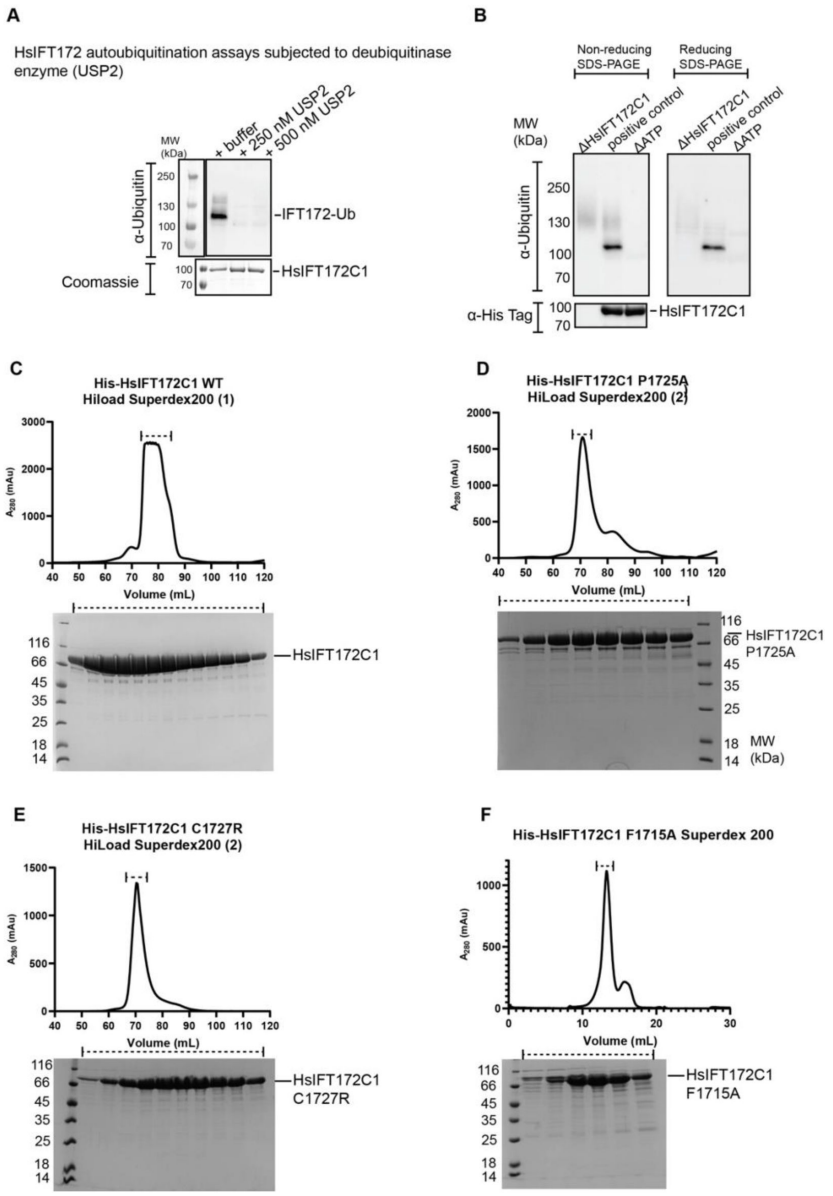

Figure S3.

Purification and auto-ubiquitination assays with HsIFT172C constructs.

(A) *In vitro* ubiquitination reactions performed with HsIFT172C1, followed by incubation with the specified concentrations of the deubiquitinase enzyme USP2 (R&D Systems # E-504-050) or buffer control. Reactions were visualized by immunostaining with (top) anti-Ubiquitin antibody and (bottom) Coomassie staining.
(B) Western blot analysis of *in vitro* ubiquitination reactions containing HsIFT172C1 after separation on a non-reducing SDS-PAGE (left) and reducing SDS-PAGE gel (right). Reactions were visualized by immunostaining with (top) anti-Ubiquitin antibody and (bottom) anti-His tag antibody. Δ indicates reaction components that were omitted in the specific reaction.
(C-F) SEC elution profiles (top) and protein composition of the denoted elution fractions analyzed by Coomassie staining post separation on SDS-PAGE (bottom) for: **(C)** HsIFT172C1 WT. **(D)** HsIFT172C1 P1725A. **(E)** HsIFT172C1 C1727R. **(F)** HsIFT172C1 F1715A. (1) and (2) denotes two different HiLoad Superdex 200 columns used to run the samples.

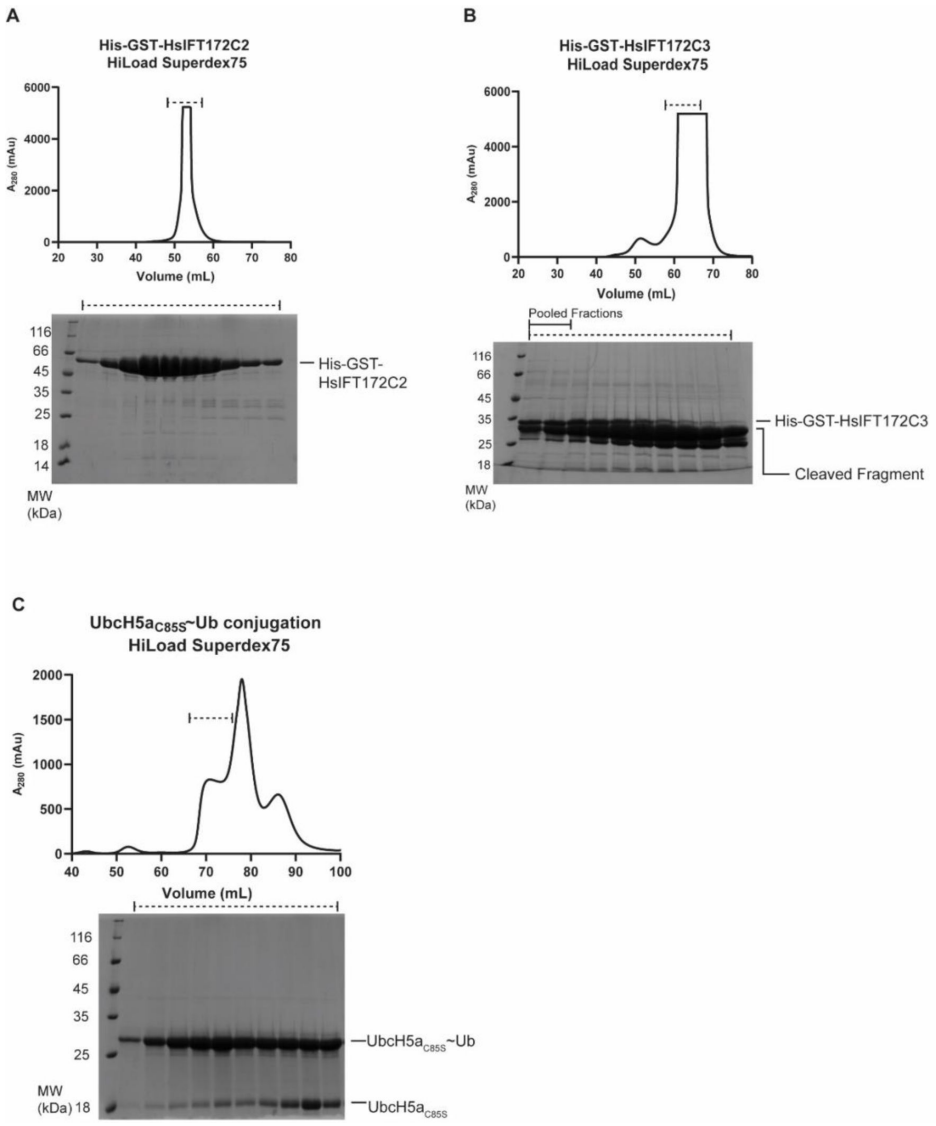

Figure S4.

Purification of GST-tagged HsIFT172 constructs and of the E2~Ub conjugate.

(A) SEC elution profile (top) and protein composition of the denoted elution fractions analyzed by Coomassie staining after separation on SDS-PAGE (bottom) for His-GST-TEV-HsIFT172C2.
(B) SEC elution profile (top) and protein composition of the denoted elution fractions (bottom) for His-GST-TEV-HsIFT172C3. A significant amount of proteolytically cleaved protein fragments was observed upon His-GST-TEV-HsIFT172C3 purification.
(C) Reaction products of an upscaled *in vitro* ubiquitin charging reaction for UbcH5a$_{C85S}$ WT conjugate separated on a SEC column (top). The denoted elution fractions were analyzed by Coomassie staining on an SDS-PAGE gel (bottom).

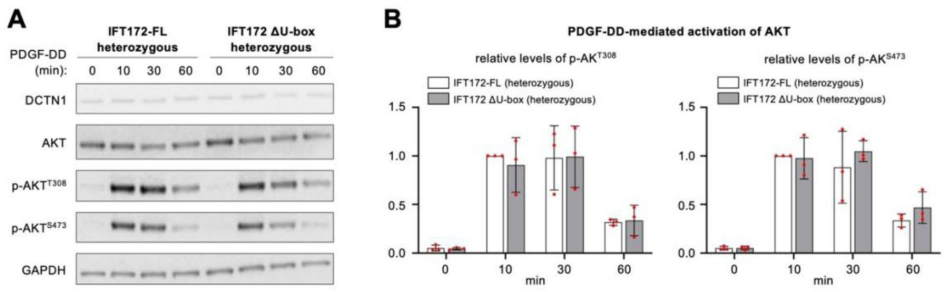

Figure S5.

Truncation of the IFT172 U-box domain impairs ciliogenesis and leads to altered TGFB signaling response in RPE1 cells.

(A) WB analysis of p-AKT levels (p-AKT^{T308} and pAKT^{S473}) in IFT172-FL (heterozygous) and IFT172ΔU-box (heterozygous) RPE1 cell lines treated with PDGF-DD ligand for the indicated time points.
(B) Quantification of p-AKT levels in panel A normalized to DCTN1 and total AKT. Error bars represent standard error of the mean.

Acknowledgements

We thank Jesper L. Karlsen and Rune T. Kidmose for assistance with biocomputing and the Institute of Molecular Biology and Genetics at Aarhus University for computing time. We also thank Michael Knop, Keith Joung, and Benjamin Kleinstiver for reagents and the Danish Molecular Biomedical Imaging Center, University of Southern Denmark, for the use of imaging equipment, supported by Novo Nordisk Foundation (NNF18SA0032928). This work was funded by grants from the Novo Nordisk Foundation (grant numbers NNF15OC00114164 and NNF23OC0085823) and the European Union's Horizon 2020 research and innovation program Marie Sklodowska-Curie Innovative Training Networks (ITN) grant 861329 to E.L.

References

1. Satir P., Christensen S. T 2007) **Overview of Structure and Function of Mammalian Cilia** *Annu. Rev. Physiol* **69**:377–400

2. Wan K. Y 2018) **Coordination of eukaryotic cilia and flagella** *Essays Biochem* **62**:829–838

3. Mill P., Christensen S. T., Pedersen L. B 2023) **Primary cilia as dynamic and diverse signalling hubs in development and disease** *Nat. Rev. Genet* **24**:421–441

4. Reiter J. F., Leroux M. R 2017) **Genes and molecular pathways underpinning ciliopathies** *Nat. Rev. Mol. Cell Biol* **18**:533–547

5. Focşa I. O., Budişteanu M., Bălgrădean M 2021) **Clinical and genetic heterogeneity of primary ciliopathies (Review)** *Int. J. Mol. Med* **48**

6. Rosenbaum J. L., Witman G. B. 2002) **Intraflagellar transport** *Nat. Rev. Mol. Cell Biol.* **3**:813–825

7. Kozminski K. G., Johnson K. A., Forscher P., Rosenbaum J. L 1993) **A motility in the eukaryotic flagellum unrelated to flagellar beating** *Proc. Natl. Acad. Sci. U. S. A* **90**:5519–5523

8. Kozminski K. G., Beech P. L., Rosenbaum J. L 1995) **The Chlamydomonas kinesin-like protein FLA10 is involved in motility associated with the flagellar membrane** *J. Cell Biol* **131**:1517–1527

9. Bhogaraju S., Weber K., Engel B. D., Lechtreck K., Lorentzen E 2014) **Getting tubulin to the tip of the cilium: One IFT train, many different tubulin cargo-binding sites?** *BioEssays* **36**:463–467

10. Lechtreck K. F 2015) **IFT-Cargo Interactions and Protein Transport in Cilia** *Trends Biochem. Sci* **40**:765–778

11. Long H., Huang K 2020) **Transport of Ciliary Membrane Proteins** *Front. Cell Dev. Biol* **7**

12. Mukhopadhyay S., et al. 2010) **TULP3 bridges the IFT-A complex and membrane phosphoinositides to promote trafficking of G protein-coupled receptors into primary cilia** *Genes Dev* **24**:2180–2193

13. Pigino G., et al. 2009) **Electron-tomographic analysis of intraflagellar transport particle trains in situ** *J. Cell Biol* **187**:135–148

14. van den Hoek H., et al. 2022) **In situ architecture of the ciliary base reveals the stepwise assembly of intraflagellar transport trains** *Science* **377**:543–548

15. Taschner M., Lorentzen E 2016) **The Intraflagellar Transport Machinery** *Cold Spring Harb. Perspect. Biol* https://doi.org/10.1101/cshperspect.a028092

16. Wingfield J. L., et al. 2017) **IFT trains in different stages of assembly queue at the ciliary base for consecutive release into the cilium** *eLife* **6**

17. Pedersen L. B., Geimer S., Rosenbaum J. L 2006) **Dissecting the Molecular Mechanisms of Intraflagellar Transport in Chlamydomonas** *Curr. Biol* **16**:450–459

18. Jordan M. A., Diener D. R., Stepanek L., Pigino G 2018) **The cryo-EM structure of intraflagellar transport trains reveals how dynein is inactivated to ensure unidirectional anterograde movement in cilia** *Nat. Cell Biol* **20**:1250–1255

19. Pazour G. J., Dickert B. L., Witman G. B 1999) **The DHC1b (DHC2) isoform of cytoplasmic dynein is required for flagellar assembly** *J. Cell Biol* **144**:473–481

20. Porter M. E., Bower R., Knott J. A., Byrd P., Dentler W 1999) **Cytoplasmic dynein heavy chain 1b is required for flagellar assembly in Chlamydomonas** *Mol. Biol. Cell* **10**:693–712

21. Eguether T., et al. 2014) **IFT27 Links the BBSome to IFT for Maintenance of the Ciliary Signaling Compartment** *Dev. Cell* **31**:279–290

22. Nachury M. V., et al. 2007) **A Core Complex of BBS Proteins Cooperates with the GTPase Rab8 to Promote Ciliary Membrane Biogenesis** *Cell* **129**:1201–1213

23. Komander D., Rape M. 2012) **The Ubiquitin Code** *Annu. Rev. Biochem.* **81**:203–229

24. Hossain D., Tsang W. Y 2019) **The role of ubiquitination in the regulation of primary cilia assembly and disassembly** *Semin. Cell Dev. Biol* **93**:145–152

25. Lv B., Stuck M. W., Desai P. B., Cabrera O. A., Pazour G. J 2021) **E3 ubiquitin ligase Wwp1 regulates ciliary dynamics of the Hedgehog receptor Smoothened** *J. Cell Biol* **220**

26. Shinde S. R., Nager A. R., Nachury M. V 2020) **Ubiquitin chains earmark GPCRs for BBSome-mediated removal from cilia** *J. Cell Biol* **219**

27. Huang K., Diener D. R., Rosenbaum J. L 2009) **The ubiquitin conjugation system is involved in the disassembly of cilia and flagella** *J. Cell Biol* **186**:601–613

28. Wang Q., Peng Z., Long H., Deng X., Huang K 2019) **Polyubiquitylation of α-tubulin at K304 is required for flagellar disassembly in Chlamydomonas** *J. Cell Sci* **132**

29. Desai P. B., Stuck M. W., Lv B., Pazour G. J 2020) **Ubiquitin links smoothened to intraflagellar transport to regulate Hedgehog signaling** *J. Cell Biol* **219**

30. Kim J., et al. 2015) **The role of ciliary trafficking in Hedgehog receptor signaling** *Sci. Signal* **8**

31. Shinde S. R., et al. 2023) **The ancestral ESCRT protein TOM1L2 selects ubiquitinated cargoes for retrieval from cilia** *Dev. Cell* **58**:677–693

32. Aslanyan M. G., et al. 2023) **A targeted multi-proteomics approach generates a blueprint of the ciliary ubiquitinome** *Front. Cell Dev. Biol* **11**

33. Chiuso F., et al. 2023) **Ubiquitylation of BBSome is required for ciliary assembly and signaling** *EMBO Rep* **24**

34. Taschner M., et al. 2016) **Intraflagellar transport proteins 172, 80, 57, 54, 38, and 20 form a stable tubulin-binding IFT-B2 complex** *EMBO J.* **35**:773–790

35. Petriman N. A., et al. 2022) **Biochemically validated structural model of the 15-subunit intraflagellar transport complex IFT-B** *EMBO J* **41**

36. Halbritter J., et al. 2013) **Defects in the IFT-B Component IFT172 Cause Jeune and Mainzer-Saldino Syndromes in Humans** *Am. J. Hum. Genet* **93**:915–925

37. Bujakowska K. M., et al. 2015) **Mutations in IFT172 cause isolated retinal degeneration and Bardet–Biedl syndrome** *Hum. Mol. Genet* **24**:230–242

38. Lucas-Herald A. K., et al. 2015) **A Case of Functional Growth Hormone Deficiency and Early Growth Retardation in a Child With IFT172 Mutations** *J. Clin. Endocrinol. Metab* **100**:1221–1224

39. Huangfu D., et al. 2003) **Hedgehog signalling in the mouse requires intraflagellar transport proteins** *Nature* **426**:83–87

40. Pedersen L. B., et al. 2005) **Chlamydomonas IFT172 Is Encoded by FLA11, Interacts with CrEB1, and Regulates IFT at the Flagellar Tip** *Curr. Biol.* **15**:262–266

41. Tsao C.-C., Gorovsky M. A 2008) **Different Effects of Tetrahymena IFT172 Domains on Anterograde and Retrograde Intraflagellar Transport** *Mol. Biol. Cell* **19**:1450–1461

42. Williamson S. M., Silva D. A., Richey E., Qin H 2012) **Probing the role of IFT particle complex A and B in flagellar entry and exit of IFT-dynein in Chlamydomonas** *Protoplasma* **249**:851–856

43. Jumper J., et al. 2021) **Highly accurate protein structure prediction with AlphaFold** *Nature* **596**:583–589

44. Evans R., et al. 2022) **Protein complex prediction with AlphaFold-Multimer** *bioRxiv* https://doi.org/10.1101/2021.10.04.463034

45. Jiang M., et al. 2023) **Human IFT-A complex structures provide molecular insights into ciliary transport** *Cell Res* **33**:288–298

46. Lacey S. E., Foster H. E., Pigino G 2023) **The molecular structure of IFT-A and IFT-B in anterograde intraflagellar transport trains** *Nat. Struct. Mol. Biol* **30**:584–593

47. Lacey S. E., Graziadei A., Pigino G 2024) **Extensive structural rearrangement of intraflagellar transport trains underpins bidirectional cargo transport** *Cell* **187**:4621–4636

48. Kloppsteck P., Ewens C. A., Förster A., Zhang X., Freemont P. S 2012) **Regulation of p97 in the ubiquitin–proteasome system by the UBX protein-family** *Biochim. Biophys. Acta BBA - Mol. Cell Res* **1823**:125–129

49. Holm L, Gáspári Z. 2020) **Using Dali for Protein Structure Comparison** *Structural Bioinformatics: Methods and Protocols* New York, NY: Springer US :29–42 https://doi.org/10.1007/978-1-0716-0270-6_3

50. Zheng N., Shabek N. 2017) **Ubiquitin Ligases: Structure, Function, and Regulation** *Annu. Rev. Biochem.* **86**:129–157

51. Ohi M. D., Vander Kooi C. W., Rosenberg J. A., Chazin W. J., Gould K. L 2003) **Structural insights into the U-box, a domain associated with multi-ubiquitination** *Nat. Struct. Mol. Biol* **10**:250–255

52. Aravind L., Koonin E. V 2000) **The U box is a modified RING finger — a common domain in ubiquitination** *Curr. Biol* **10**:R132–R134

53. Hatakeyama S., Yada M., Matsumoto M., Ishida N., Nakayama K.-I 2001) **U Box Proteins as a New Family of Ubiquitin-Protein Ligases *** *J. Biol. Chem* **276**:33111–33120

54. Özkan E., Yu H., Deisenhofer J. 2005) **Mechanistic insight into the allosteric activation of a ubiquitin-conjugating enzyme by RING-type ubiquitin ligases** *Proc. Natl. Acad. Sci* **102**:18890–18895

55. Dou H., Buetow L., Sibbet G. J., Cameron K., Huang D. T 2012) **BIRC7–E2 ubiquitin conjugate structure reveals the mechanism of ubiquitin transfer by a RING dimer** *Nat. Struct. Mol. Biol* **19**:876–883

56. Plechanovová A., Jaffray E. G., Tatham M. H., Naismith J. H., Hay R. T 2012) **Structure of a RING E3 ligase and ubiquitin-loaded E2 primed for catalysis** *Nature* **489**:115–120

57. Soss S. E., Klevit R. E., Chazin W. J 2013) **Activation of UbcH5c∼Ub is the result of a shift in interdomain motions of the conjugate bound to U-box E3 ligase E4B** *Biochemistry* **52**:2991–2999

58. Buetow L., Huang D. T 2016) **Structural insights into the catalysis and regulation of E3 ubiquitin ligases** *Nat. Rev. Mol. Cell Biol* **17**:626–642

59. Dou H., et al. 2012) **Structural basis for autoinhibition and phosphorylation-dependent activation of c-Cbl** *Nat. Struct. Mol. Biol* **19**:184–192

60. Trempe J.-F., et al. 2013) **Structure of parkin reveals mechanisms for ubiquitin ligase activation** *Science* **340**:1451–1455

61. Moura T. R. de, et al. 2018) **Prp19/Pso4 Is an Autoinhibited Ubiquitin Ligase Activated by Stepwise Assembly of Three Splicing Factors** *Mol. Cell* **69**:979–992

62. de Bie P., Ciechanover A 2011) **Ubiquitination of E3 ligases: self-regulation of the ubiquitin system via proteolytic and non-proteolytic mechanisms** *Cell Death Differ* **18**:1393–1402

63. Hoeller D., et al. 2007) **E3-Independent Monoubiquitination of Ubiquitin-Binding Proteins** *Mol. Cell* **26**:891–898

64. Garcia-Barcena C., Osinalde N., Ramirez J., Mayor U 2020) **How to Inactivate Human Ubiquitin E3 Ligases by Mutation** *Front. Cell Dev. Biol* **8**

65. Zheng N., Wang P., Jeffrey P. D., Pavletich N. P 2000) **Structure of a c-Cbl–UbcH7 Complex: RING Domain Function in Ubiquitin-Protein Ligases** *Cell* **102**:533–539

66. Middleton A. J., Budhidarmo R., Day C. L., Ashkenazi A., Wells J. A., Yuan J. 2014) **Chapter Ten - Use of E2∼Ubiquitin Conjugates for the Characterization of Ubiquitin Transfer by RING E3 Ligases Such as the Inhibitor of Apoptosis Proteins** *Methods in Enzymology* Academic Press :243–263

67. Gundogdu M., Walden H 2019) **Structural basis of generic versus specific E2–RING E3 interactions in protein ubiquitination** *Protein Sci* **28**:1758–1770

68. Levin I., et al. 2010) **Identification of an unconventional E3 binding surface on the UbcH5 ~ Ub conjugate recognized by a pathogenic bacterial E3 ligase** *Proc. Natl. Acad. Sci* **107**:2848–2853

69. Xu Z., et al. 2008) **Interactions between the quality control ubiquitin ligase CHIP and ubiquitin conjugating enzymes** *BMC Struct. Biol* **8**

70. Pruski M., et al. 2019) **Roles for IFT172 and Primary Cilia in Cell Migration, Cell Division, and Neocortex Development** *Front. Cell Dev. Biol* **7**

71. Clement C. A., et al. 2013) **TGF-β Signaling Is Associated with Endocytosis at the Pocket Region of the Primary Cilium** *Cell Rep* **3**:1806–1814

72. Doganli C., et al. 2024) **TAK1 operates at the primary cilium in non-canonical TGFB/BMP signaling to control heart development** *bioRxiv* https://doi.org/10.1101/2024.05.06.592628

73. Nielsen B. S., et al. 2015) **PDGFRβ and oncogenic mutant PDGFRα D842V promote disassembly of primary cilia through a PLCγ- and AURKA-dependent mechanism** *J. Cell Sci* **128**:3543–3549

74. Wang Q., et al. 2018) **Membrane association and remodeling by intraflagellar transport protein IFT172** *Nat. Commun* **9**

75. Kassenbrock C. K., Anderson S. M 2004) **Regulation of Ubiquitin Protein Ligase Activity in c-Cbl by Phosphorylation-induced Conformational Change and Constitutive Activation by Tyrosine to Glutamate Point Mutations*** *J. Biol. Chem* **279**:28017–28027

76. Hornbeck P. V., et al. 2015) **PhosphoSitePlus, 2014: mutations, PTMs and recalibrations** *Nucleic Acids Res* **43**:D512–D520

77. Bomar M. G., Pai M.-T., Tzeng S.-R., Li S. S.-C., Zhou P 2007) **Structure of the ubiquitin-binding zinc finger domain of human DNA Y-polymerase η** *EMBO Rep* **8**:247–251

78. Guo X., Wang X.-F 2009) **Signaling cross-talk between TGF-β/BMP and other pathways** *Cell Res* **19**:71–88

79. Heldin C.-H., Moustakas A 2016) **Signaling Receptors for TGF-β Family Members** *Cold Spring Harb. Perspect. Biol* **8**

80. Zhang Y. E 2009) **Non-Smad pathways in TGF-β signaling** *Cell Res* **19**:128–139

81. Gibson D. G., et al. 2009) **Enzymatic assembly of DNA molecules up to several hundred kilobases** *Nat. Methods* **6**:343–345

82. Craige B., Brown J. M., Witman G. B 2013) **Isolation of Chlamydomonas Flagella** *Curr. Protoc. Cell Biol* **59**:3–3

83. Kabsch W. 2010) **XDS** *Acta Crystallogr. D Biol. Crystallogr.* **66**:125–132

84. Winn M. D., et al. 2011) **Overview of the CCP4 suite and current developments** *Acta Crystallogr. D Biol. Crystallogr* **67**:235–242

85. McCoy A. J., et al. 2007) **Phaser crystallographic software** *J. Appl. Crystallogr.* **40**:658–674

86. Liebschner D., et al. 2019) **Macromolecular structure determination using X-rays, neutrons and electrons: recent developments in Phenix** *Acta Crystallogr. Sect. Struct. Biol* **75**:861–877

87. Hughes C. S., et al. 2019) **Single-pot, solid-phase-enhanced sample preparation for proteomics experiments** *Nat. Protoc* **14**:68–85

88. Kuhns S., et al. 2024) **Endogenous Tagging of Ciliary Genes in Human RPE1 Cells for Live-Cell Imaging** *Methods Mol Biol* **2725**:147–166

89. Fueller J., et al. 2020) **CRISPR-Cas12a-assisted PCR tagging of mammalian genes** *J Cell Biol* **219**

90. Kleinstiver B. P., et al. 2019) **Engineered CRISPR-Cas12a variants with increased activities and improved targeting ranges for gene, epigenetic and base editing** *Nat Biotechnol* **37**:276–282

91. Riesenberg S., et al. 2019) **Simultaneous precise editing of multiple genes in human cells** *Nucleic Acids Res* **47**

92. Schindelin J., et al. 2012) **Fiji: an open-source platform for biological-image analysis** *Nat Methods* **9**:676–682

93. Emsley P., Lohkamp B., Scott W. G., Cowtan K. 2010) **Features and development of Coot** *Acta Crystallogr D Biol Crystallogr* **66**:486–501

Author information

Nevin K Zacharia
Department of Molecular Biology and Genetics, Aarhus University, Aarhus, Denmark

Stefanie Kuhns
Department for Biochemistry and Molecular Biology, University of Southern Denmark, Odense, Denmark

Niels Boegholm
Department of Molecular Biology and Genetics, Aarhus University, Aarhus, Denmark

Anni Christensen
Department of Molecular Biology and Genetics, Aarhus University, Aarhus, Denmark

Jiaolong Wang
Department of Molecular Biology and Genetics, Aarhus University, Aarhus, Denmark

Narcis A Petriman
Department of Molecular Biology and Genetics, Aarhus University, Aarhus, Denmark, Department of Biology, University of Copenhagen, Copenhagen, Denmark

Anna Lorentzen
Department of Molecular Biology and Genetics, Aarhus University, Aarhus, Denmark

Jindriska L Fialova
Department of Biology, University of Copenhagen, Copenhagen, Denmark

Lucie Menguy
Laboratory of Hereditary and Kidney diseases, Institut Imagine, Paris, France

Sophie Saunier
Laboratory of Hereditary and Kidney diseases, Institut Imagine, Paris, France

Soren T Christensen
Department of Biology, University of Copenhagen, Copenhagen, Denmark

Jens S Andersen
Department for Biochemistry and Molecular Biology, University of Southern Denmark, Odense, Denmark

Sagar Bhogaraju
European Molecular Biology Laboratory, Grenoble, France

For correspondence: bhogaraju@embl.fr

Esben Lorentzen
Department of Molecular Biology and Genetics, Aarhus University, Aarhus, Denmark

For correspondence: el@mbg.au.dk

Editors

Reviewing Editor
Junmin Pan
Tsinghua University, Beijing, China

Senior Editor
Amy Andreotti
Iowa State University, Ames, United States of America

Reviewer #1 (Public review):

Summary:

Zacharia and colleagues investigate the role of the C-terminus of IFT172 (IFT172c), a component of the IFT-B subcomplex. IFT172 is required for proper ciliary trafficking and mutations in its C-terminus are associated with skeletal ciliopathies. The authors begin by performing a pull-down to identify binding partners of His-tagged CrIFT172968-C in Chlamydomonas reinhardtii flagella. Interactions with three candidates (IFT140, IFT144, and a UBX-domain containing protein) are validated by AlphaFold Multimer with the IFT140 and IFT144 predictions in agreement with published cryo-ET structures of anterograde and retrograde IFT trains. They present a crystal structure of IFT172c and find that a part of the C-terminal domain of IFT172 resembles the fold of a non-canonical U-box domain. As U-box domains typically function to bind ubiquitin-loaded E2 enzymes, this discovery stimulates the authors to investigate the ubiquitin-binding and ubiquitination properties of IFT172c. Using in vitro ubiquitination assays with truncated IFT172c constructs, the authors demonstrate

partial ubiquitination of IFT172c in the presence of the E2 enzyme UBCH5A. The authors also show a direct interaction of IFT172c with ubiquitin chains in vitro. Finally, the authors demonstrate that deletion of the U-box-like subdomain of IFT172 impairs ciliogenesis and TGFbeta signaling in RPE1 cells.

However, some of the conclusions of this paper are only partially supported by the data, and presented analyses are potentially governed by in vitro artifacts. In particular, the data supporting autoubiquitination and ubiquitin-binding are inconclusive. Without further evidence supporting a ubiquitin-binding role for the C-terminus, the title is potentially misleading.

Strengths:

(1) The pull-down with IFT172 C-terminus from C. reinhardtii cilia lysates is well performed and provides valuable insights into its potential roles.

(2) The crystal structure of the IFT172 C-terminus is of high quality.

(3) The presented AlphaFold-multimer predictions of IFT172c:IFT140 and IFT172c:IFT144 are convincing and agree with experimental cryo-ET data.

Weaknesses:

(1) The crystal structure of HsIFT172c reveals a single globular domain formed by the last three TPR repeats and C-terminal residues of IFT172. However, the authors subdivide this globular domain into TPR, linker, and U-box-like regions that they treat as separate entities throughout the manuscript. This is potentially misleading as the U-box surface that is proposed to bind ubiquitin or E2 is not surface accessible but instead interacts with the TPR motifs. They justify this approach by speculating that the presented IFT172c structure represents an autoinhibited state and that the U-box-like domain can become accessible following phosphorylation. However, additional evidence supporting the proposed autoinhibited state and the potential accessibility of the U-box surface following phosphorylation is needed, as it is not tested or supported by the current data.

(2) While in vitro ubiquitination of IFT172 has been demonstrated, in vivo evidence of this process is necessary to support its physiological relevance.

(3) The authors describe IFT172 as being autoubiquitinated. However, the identified E2 enzymes UBCH5A and UBCH5B can both function in E3-independent ubiquitination (as pointed out by the authors) and mediate ubiquitin chain formation in an E3-independent manner in vitro (see ubiquitin chain ladder formation in Figure 3A). In addition, point mutation of known E3-binding sites in UBCH5A or TPR/U-box interface residues in IFT172 has no effect on the mono-ubiquitination of IFT172c1. Together, these data suggest that IFT172 is an E3-independent substrate of UBCH5A in vitro. The authors should state this possibility more clearly and avoid terminology such as "autoubiquitination" as it implies that IFT172 is an E3 ligase, which is misleading. Similarly, statements on page 10 and elsewhere are not supported by the data (e.g. "the low in vitro ubiquitination activity exhibited by IFT172" and "ubiquitin conjugation occurring on HsIFT172C1 in the presence of UBCH5A, possibly in coordination with the IFT172 U-box domain").

(4) Related to the above point, the conclusion on page 11, that mono-ubiquitination of IFT172 is U-box-independent while polyubiquitination of IFT172 is U-box-dependent appears implausible. The authors should consider that UBCH5A is known to form free ubiquitin chains in vitro and structural rearrangements in F1715A/C1725R variants could render additional ubiquitination sites or the monoubiquitinated form of IFT172 inaccessible/unfavorable for further processing by UBCH5A.

(5) Identification of the specific ubiquitination site(s) within IFT172 would be valuable as it would allow targeted mutation to determine whether the ubiquitination of IFT172 is physiologically relevant. Ubiquitination of the C1 but not the C2 or C3 constructs suggests that the ubiquitination site is located in TPRs ranging from residues 969-1470. Could this region of TPR repeats (lacking the IFT172C3 part) suffice as a substrate for UBCH5A in ubiquitination assays?

(6) The discrepancy between the molecular weight shifts observed in anti-ubiquitin Western blots and Coomassie-stained gels is noteworthy. The authors show the appearance of a mono-ubiquitinated protein of ~108 kDa in anti-ubiquitin Western blots. However, this molecular weight shift is not observed for total IFT172 in the corresponding Coomassie-stained gels (Figures 3B, D, F). Surprisingly, this MW shift is visible in an anti-His Western blot of a ubiquitination assay (Fig 3C). Together, this raises the concern that only a small fraction of IFT172 is being modified with ubiquitin. Quantification of the percentage of ubiquitinated IFT172 in the in vitro experiments could provide helpful context.

(7) The authors propose that IFT172 binds ubiquitin and demonstrate that GST-tagged HsIFT172C2 or HsIFT172C3 can pull down tetra-ubiquitin chains. However, ubiquitin is known to be "sticky" and to have a tendency for weak, nonspecific interactions with exposed hydrophobic surfaces. Given that only a small proportion of the ubiquitin chains bind in the pull-down, specific point mutations that identify the ubiquitin-binding site are required to convincingly show the ubiquitin binding of IFT172.

(8) The authors generated structure-guided mutations based on the predicted Ub-interface and on the TPR/U-box interface and used these for the ubiquitination assays in Fig 3. These same mutations could provide valuable insights into ubiquitin binding assays as they may disrupt or enhance ubiquitin binding (by relieving "autoinhibition"), respectively. Surprisingly, two of these sites are highlighted in the predicted ubiquitin-binding interface (F1715, I1688; Figure 4E) but not analyzed in the accompanying ubiquitin-binding assays in Figure 4.

(9) If IFT172 is a ubiquitin-binding protein, it might be expected that the pull-down experiments in Figure S1 would identify ubiquitin, ubiquitinated proteins, or E2 enzymes. These were not observed, raising doubt that IFT172 is a ubiquitin-binding protein.

(10) The cell-based experiments demonstrate that the U-box-like region is important for the stability of IFT172 but does not demonstrate that the effect on the TGFb pathway is due to the loss of ubiquitin-binding or ubiquitination activity of IFT172.

(11) The challenges in experimentally validating the interaction between IFT172 and the UBX-domain-containing protein are understandable. Alternative approaches, such as using single domains from the UBX protein, implementing solubilizing tags, or disrupting the predicted binding interface in Chlamydomonas flagella pull-downs, could be considered. In this context, the conclusion on page 7 that "The uncharacterized UBX-domain-containing protein was validated by AF-M as a direct IFT172 interactor" is incorrect as a prediction of an interaction interface with AF-M does not validate a direct interaction per se.

https://doi.org/10.7554/eLife.104906.1.sa3

Reviewer #2 (Public review):

Summary:

Cilia are antenna-like extensions projecting from the surface of most vertebrate cells. Protein transport along the ciliary axoneme is enabled by motor protein complexes with multimeric

so-called IFT-A and IFT-B complexes attached. While the components of these IFT complexes have been known for a while, precise interactions between different complex members, especially how IFT-A and IFT-B subcomplexes interact, are still not entirely clear. Likewise, the precise underlying molecular mechanism in human ciliopathies resulting from IFT dysfunction has remained elusive.

Here, the authors investigated the structure and putative function of the to-date poorly characterised C-terminus of IFT-B complex member IFT172 using alpha-fold predictions, crystallography and biochemical analyses including proteomics analyses followed by mass spectrometry, pull-down assays, and TGFbeta signalling analyses using chlamydomonas flagellae and RPE cells. The authors hereby provide novel insights into the crystal structure of IFT172 and identify novel interaction sites between IFT172 and the IFT-A complex members IFT140/IFT144. They suggest a U-box-like domain within the IFT172 C-terminus could play a role in IFT172 auto-ubiquitination as well as for TGFbeta signalling regulation.

As a number of disease-causing IFT72 sequence variants resulting in mammalian ciliopathy phenotypes in IFT172 have been previously identified in the IFT172 C-terminus, the authors also investigate the effects of such variants on auto-ubiquitination. This revealed no mutational effect on mono-ubiquitination which the authors suggest could be independent of the U-box-like domain but reduced overall IFT172 ubiquitination.

Strengths:

The manuscript is clear and well written and experimental data is of high quality. The findings provide novel insights into IFT172 function, IFT complex-A and B interactions, and they offer novel potential mechanisms that could contribute to the phenotypes associated with IFT172 C-terminal ciliopathy variants.

Weaknesses:

Some suggestions/questions are included in the comments to the authors below.

https://doi.org/10.7554/eLife.104906.1.sa2

Reviewer #3 (Public review):

Summary:

Zacharia et al report on the molecular function of the C-terminal domain of the intraflagellar transport IFT-B complex component IFT172 by structure determination and biochemical in vitro and cell culture-based assays. The authors identify an IFT-A binding site that mediates a mutually exclusive interaction to two different IFT-A subunits, IFT144 and IFT140, consistent with interactions suggested in anterograde and retrograde IFT trains by previous cryo-electron tomography studies. Additionally, the authors identify a U-box-like domain that binds ubiquitin and conveys ubiquitin conjugation activity in the presence of the UbcH5a E2 enzyme in vitro. RPE1 cell lines that lack the U-box domain show a reduction in ciliation rate with shorter cilia, and heterozygous cells manifest TGF-beta signaling defects, suggesting an involvement of the U-box domain in cilium-dependent signaling.

Strengths:

(1) The structural analyses of the C-terminal domain of IFT172 combine crystallography with structure prediction using state-of-the-art algorithms, which gives high confidence in the presented protein structures. The structure-based predictions of protein interactions are validated by further biochemical experiments to assess the specific binding of the IFT172 C-terminal domains with other proteins.

(2) The finding that the IFT172 C-terminus interactions with the IFT-A components IFT140 and IFT144 appear mutually exclusive confirm a suggested role in mediating the binding of IFT-B to IFT-A in anterograde and retrograde IFT trains, which is of very high scientific value.

(3) The suggested molecular mechanism of IFT train coordination explains previous findings in Chlamydomonas IFT172 mutants, in particular an IFT172 mutant that appeared defective in retrograde IFT, as well as mutations identified in ciliopathy patients.

(4) The identification of other IFT172 interactors by unbiased mass spectrometry-based proteomics is very exciting. Analysis of stoichiometries between IFT components suggests that these interactors could be part of IFT trains, either as cargos or additional components that may fulfill interesting functions in cilia and flagella.

(5) The authors unexpectedly identify a U-box-like fold in the IFT172 C-terminus and thoroughly dissect it by sequence and mutational analyses to reveal unexpected ubiquitin binding and potential intrinsic ubiquitination activity.

(6) The overall data quality is very high. The use of IFT172 proteins from different organisms suggests a conserved function.

Weaknesses:

(1) Interaction studies were carried out by pulldown experiments, which identified more IFT172 interaction partners. Whether these interactions can be seen in living cells remains to be elucidated in subsequent studies.

(2) The cell culture-based experiments in the IFT172 mutants are exciting and show that the U-box domain is important for protein stability and point towards involvement of the U-box domain in cellular signaling processes. However, the characterization of the generated cell lines falls behind the very rigorous analysis of other aspects of this work.

Overall, the authors achieved to characterize an understudied protein domain of the ciliary intraflagellar transport machinery and gained important molecular insights into its role in primary cilia biology, beyond IFT. By identifying an unexpected functional protein domain and novel interaction partners the work makes an important contribution to further our understanding of how ciliary processes might be regulated by ubiquitination on a molecular level. Based on this work it will be important for future studies in the cilia community to consider direct ubiquitin binding by IFT complexes.

Conceptually, the study highlights that protein transport complexes can exhibit additional intrinsic structural features for potential auto-regulatory processes. Moreover, the study adds to the functional diversity of small U-box and ubiquitin-binding domains, which will be of interest to a broader cell biology and structural biology audience.

Additional comments:

The authors investigate the consequences of the U-box deletion on ciliary TGF-beta signaling. While a cilium-dependent effect of TGF-beta signaling on the phosphorylation of SMAD2 has been demonstrated, the precise function of cilia in AKT signaling has not been fully established in the field. Therefore, the relevance of this finding is somewhat unclear. It may help to discuss relevant literature on the topic, such as Shim et al., PNAS, 2020.

https://doi.org/10.7554/eLife.104906.1.sa1

Author response:

> ***Reviewer #1:***
>
> *Weaknesses:*
>
> *(1) The crystal structure of HsIFT172c reveals a single globular domain formed by the last three TPR repeats and C-terminal residues of IFT172. However, the authors subdivide this globular domain into TPR, linker, and U-box-like regions that they treat as separate entities throughout the manuscript. This is potentially misleading as the U-box surface that is proposed to bind ubiquitin or E2 is not surface accessible but instead interacts with the TPR motifs. They justify this approach by speculating that the presented IFT172c structure represents an autoinhibited state and that the U-box-like domain can become accessible following phosphorylation. However, additional evidence supporting the proposed autoinhibited state and the potential accessibility of the U-box surface following phosphorylation is needed, as it is not tested or supported by the current data.*

We thank the reviewer for this comment. IFT172C contains TPR region and Ubox-like region which are admittedly tightly bound to each other. While there is a possibility that this region functions and exists as one domain, below are the reasons why we chose to classify these regions as two different domains.

(1) TPR and Ubox-like regions are two different structural classes

(2) TPR region is linked to Ubox-like region via a long linker which seems poised to regulate the relative movement between these regions.

(3) Many ciliopathy mutations are mapped to the interface of TPR region and the Ubox region hinting at a regulatory mechanism governed by this interface.

> *(2) While in vitro ubiquitination of IFT172 has been demonstrated, in vivo evidence of this process is necessary to support its physiological relevance.*

We thank the reviewer for this comment. We are currently working on identifying the substrates of IF172 to reveal the physiological relevant of its ubiquitination activity.

> *(3) The authors describe IFT172 as being autoubiquitinated. However, the identified E2 enzymes UBCH5A and UBCH5B can both function in E3-independent ubiquitination (as pointed out by the authors) and mediate ubiquitin chain formation in an E3-independent manner in vitro (see ubiquitin chain ladder formation in Figure 3A). In addition, point mutation of known E3-binding sites in UBCH5A or TPR/U-box interface residues in IFT172 has no effect on the mono-ubiquitination of IFT172c1. Together, these data suggest that IFT172 is an E3-independent substrate of UBCH5A in vitro. The authors should state this possibility more clearly and avoid terminology such as "autoubiquitination" as it implies that IFT172 is an E3 ligase, which is misleading. Similarly, statements on page 10 and elsewhere are not supported by the data (e.g. "the low in vitro ubiquitination activity exhibited by IFT172" and "ubiquitin conjugation occurring on HsIFT172C1 in the presence of UBCH5A, possibly in coordination with the IFT172 U-box domain").*

We now consider this possibility and tone down our statements about the autoubiquitination activity of IFT172 in a revised version of the manuscript.

> *(4) Related to the above point, the conclusion on page 11, that mono-ubiquitination of IFT172 is U-box-independent while polyubiquitination of IFT172 is U-box-dependent appears implausible. The authors should consider that UBCH5A is known to form free*

> *ubiquitin chains in vitro and structural rearrangements in F1715A/C1725R variants could render additional ubiquitination sites or the monoubiquitinated form of IFT172 inaccessible/unfavorable for further processing by UBCH5A.*

We now consider this possibility and tone down our statements about the autoubiquitination activity of IFT172 in the conclusion on pg. 11.

> *(5) Identification of the specific ubiquitination site(s) within IFT172 would be valuable as it would allow targeted mutation to determine whether the ubiquitination of IFT172 is physiologically relevant. Ubiquitination of the C1 but not the C2 or C3 constructs suggests that the ubiquitination site is located in TPRs ranging from residues 969-1470. Could this region of TPR repeats (lacking the IFT172C3 part) suffice as a substrate for UBCH5A in ubiquitination assays?*

We thank the reviewer for raising this important point about ubiquitination site identification. While not included in our manuscript, we did perform mass spectrometry analysis of ubiquitination sites using wild-type IFT172 and several mutants (P1725A, C1727R, and F1715A). As shown in the figure below, we detected multiple ubiquitination sites across these constructs. The wild-type protein showed ubiquitination at positions K1022, K1237, K1271, and K1551, while the mutants displayed slightly different patterns of modification. However, we should note that the MS intensity signals for these ubiquitinated peptides were relatively low compared to unmodified peptides, making it difficult to draw strong conclusions about site specificity or physiological relevance.

Author response image 1.

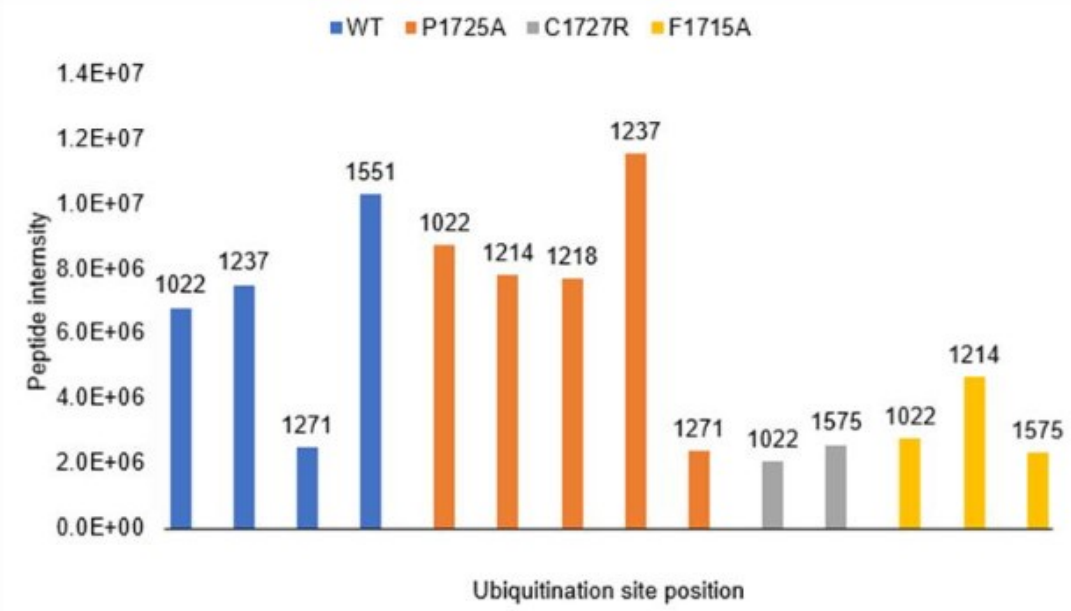

These results align with the reviewer's suggestion that ubiquitination occurs within the TPR-containing region. However, given the technical limitations of the MS analysis and the potential for E3-independent ubiquitination by UBCH5A, we have taken a conservative approach in interpreting these findings.

> *(6) The discrepancy between the molecular weight shifts observed in anti-ubiquitin Western blots and Coomassie-stained gels is noteworthy. The authors show the appearance of a mono-ubiquitinated protein of ~108 kDa in anti-ubiquitin Western blots.*

> *However, this molecular weight shift is not observed for total IFT172 in the corresponding Coomassie-stained gels (Figures 3B, D, F). Surprisingly, this MW shift is visible in an anti-His Western blot of a ubiquitination assay (Fig 3C). Together, this raises the concern that only a small fraction of IFT172 is being modified with ubiquitin. Quantification of the percentage of ubiquitinated IFT172 in the in vitro experiments could provide helpful context.*

We do acknowledge in the manuscript is that the conjugation of ubiquitins to IFT172C is weak (Page 16). Future experiments of identification of potential substrates and its implications in ciliary regulation will provide further context to our in vitro ubiquitination experiments.

> *(7) The authors propose that IFT172 binds ubiquitin and demonstrate that GST-tagged HsIFT172C2 or HsIFT172C3 can pull down tetra-ubiquitin chains. However, ubiquitin is known to be "sticky" and to have a tendency for weak, nonspecific interactions with exposed hydrophobic surfaces. Given that only a small proportion of the ubiquitin chains bind in the pull-down, specific point mutations that identify the ubiquitin-binding site are required to convincingly show the ubiquitin binding of IFT172.*
>
> *(8) The authors generated structure-guided mutations based on the predicted Ub-interface and on the TPR/U-box interface and used these for the ubiquitination assays in Fig 3. These same mutations could provide valuable insights into ubiquitin binding assays as they may disrupt or enhance ubiquitin binding (by relieving "autoinhibition"), respectively. Surprisingly, two of these sites are highlighted in the predicted ubiquitin-binding interface (F1715, I1688; Figure 4E) but not analyzed in the accompanying ubiquitin-binding assays in Figure 4.*

We agree that these mutations could provide insights into ubiquitin binding by IFT172. We are currently pursuing further mutagenesis studies on the IFT172-Ub interface based on the AF model. We however have evaluated the ubiquitin binding activity of the mutant F1715A using similar pulldowns, which showed no significant impact for the mutation on the ubiquitin binding activity of IFT172. We are yet to evaluate the impact of alternate amino acid substitutions at these positions. The I1688 mutants we cloned could not be expressed in soluble form, thus could not be used for testing in ubiquitination activity or ubiquitin binding assays.

> *(9) If IFT172 is a ubiquitin-binding protein, it might be expected that the pull-down experiments in Figure S1 would identify ubiquitin, ubiquitinated proteins, or E2 enzymes. These were not observed, raising doubt that IFT172 is a ubiquitin-binding protein.*

It is likely that IFT172 only binds ubiquitin with low affinity as indicated by our in vitro pulldowns and the AF interface. In our pull down experiment performed using the Chlamy flagella extracts, we have used extensive washes to remove non-specific interactors. This might have also excluded the identification of weak but bona fide interactors of IFT172. Additionally, we have not used any ubiquitination preserving reagents such as NEM in our pulldown buffers, exposing the cellular ubiquitinated proteins to DUB mediated proteolysis further preventing their identification in our pulldown/MS experiment.

> *(10) The cell-based experiments demonstrate that the U-box-like region is important for the stability of IFT172 but does not demonstrate that the effect on the TGFb pathway is due to the loss of ubiquitin-binding or ubiquitination activity of IFT172.*

We acknowledge that our current data cannot distinguish whether the TGFβ pathway defects arise from general protein instability or from specific loss of ubiquitin-related functions. Our experiments demonstrate that the U-box-like region is required for both IFT172 stability and

proper TGFβ signaling, but we agree that establishing a direct mechanistic link between these phenomena would require additional evidence. We will revise our discussion to more clearly acknowledge this limitation in our current understanding of the relationship between IFT172's U-box region and TGFβ pathway regulation.

> *(11) The challenges in experimentally validating the interaction between IFT172 and the UBX-domain-containing protein are understandable. Alternative approaches, such as using single domains from the UBX protein, implementing solubilizing tags, or disrupting the predicted binding interface in Chlamydomonas flagella pull-downs, could be considered. In this context, the conclusion on page 7 that "The uncharacterized UBX-domain-containing protein was validated by AF-M as a direct IFT172 interactor" is incorrect as a prediction of an interaction interface with AF-M does not validate a direct interaction per se.*

We agree with the reviewer that our AlphaFold-Multimer (AF-M) predictions alone do not constitute experimental validation of a direct interaction. We appreciate the reviewer's understanding of the technical challenges in validating this interaction experimentally. We will revise our text to more precisely state that "The uncharacterized UBX-domain-containing protein was validated by AF-M as a potential direct IFT172 interactor" and will discuss the AF-M predictions as computational evidence that suggests, but does not prove, a direct interaction. This more accurately reflects the current state of our understanding of this potential interaction.

> ***Reviewer #3:***
>
> *Weaknesses:*
>
> *(1) Interaction studies were carried out by pulldown experiments, which identified more IFT172 interaction partners. Whether these interactions can be seen in living cells remains to be elucidated in subsequent studies.*

We agree with the reviewer that validation of protein-protein interactions in living cells provides important physiological context. While our pulldown experiments have identified several promising interaction partners and the AF-M predictions provide computational support for these interactions, we acknowledge that demonstrating these interactions in vivo would strengthen our findings. However, we believe our current biochemical and structural analyses provide valuable insights into the molecular basis of IFT172's interactions, laying important groundwork for future cell-based studies.

> *(2) The cell culture-based experiments in the IFT172 mutants are exciting and show that the U-box domain is important for protein stability and point towards involvement of the U-box domain in cellular signaling processes. However, the characterization of the generated cell lines falls behind the very rigorous analysis of other aspects of this work.*

We thank the reviewer for noting that the characterization of our cell lines could be more rigorous. In the revised manuscript, we will provide additional characterization of the cell lines, including detailed sequencing information and validation data for the IFT172 mutants. This will bring the documentation of our cell-based experiments up to the same standard as other aspects of our work.

https://doi.org/10.7554/eLife.104906.1.sa0